A MAJOR PROJECT REPORT ON

"COMPUTATIONAL INVESTIGATION OF GAS TURBINE BLADE COOLING"

BY

Rajesh K. Gupta

(University Roll No. 10235)

Under the able guidance of Dr. Samsher & Dr. B. D. Pathak

Department of Mechanical Engineering,

Delhi College of Engineering, University of Delhi

Session 2006-08

Candidate's Declaration

I, hereby, declare that the major project report on "**COMPUTATIONAL INVESTIGATION OF GAS TURBINE BLADE COOLING"** for the partial fulfillment of the award of the degree of '**Master of Engineering'** with the specialization in "**Thermal Engineering"** is the authentic record of my own work carried out under the supervision of **Dr. Samsher & Dr. B. D. Pathak,** Department of Mechanical Engineering, Delhi College of Engineering, University of Delhi. I have not submitted the matter in this project for the award of any degree or any other purpose whatsoever.

Rajesh K. Gupta
(College Roll No. 07/THR/2006)
University Roll No. 10235

Certificate

This is to certify that the above statements made by Rajesh K. Gupta are true to the best of my knowledge and belief.

Dr. Samsher
Assitant Professor
Dept. of Mechanical Engg.
Delhi college of Engg.

Dr. B. D. Pathak
Professor
Dept. of Mechanical Engg.
Delhi College of Engg.

Acknowledgement

It is a great pleasure to have the opportunity to extend my heartiest felt gratitude to everybody who helped me throughout the course of this seminar. It is distinct pleasure to express my deep sense of gratitude and indebtedness to my teacher **Dr. Samsher & Dr. B. D. Pathak, d**epartment of Mechanical Engineering, Delhi College of Engineering, for his invaluable guidance, encouragement and patient review. Their continuous inspiration only has made me complete this project.

I would also like to take this opportunity to present my sincere regards to my teachers for their kind support and encouragement.

I am thankful to my friends and classmates for their unconditional support and motivation for this project.

Rajesh K. Gupta

College Roll No. 07/thr/06

University Roll. No. 10235

ABSTRACT

The nozzle guide vanes are subjected to the highest temperature of the gas coming out of the combustor in a gas turbine engine. One method used to cool the vanes are to use rows of film cooling holes to inject cooled air bled from the compressor lower pressure stage. The main purpose of this project is to investigate computationally the film cooling phenomena in gas turbine vane cascade. Computational fluid dynamics (CFD) has been used for the simulation of the aerothermodynamics of film cooling. Two types of holes have been investigated; simple cylindrical hole and fan-shaped hole. Initially a three dimensional cascade with film cooling holes and plenum chamber was developed, but due to the limitation of computational resources the model was aborted and then a two dimension model was investigated. The modeling of the domain has been done in Gambit 2.0.1. Unstructured grid (quad-pave scheme) was used for the solver. The solver used for the CFD simulation was Fluent^{TM} 6.0.1. RNG K-Ɛ turbulence model with standard wall function was selected for the simulation.

For various blowing ratios, the temperature and flow field are predicted for both types of hole. The study of the effect of turbulence model was also done. It was found that as the blowing ratio increased, film cooling performance improved for both cylindrical as well as fan-shaped holes.

LIST OF TABLES: -

LIST OF SYMBOLS: -

κ- turbulent kinetic energy

ε - Dissipation of turbulent kinetic energy

v – Kinematic viscosity

f – near wall anisotropy correction factor

ρ_c – density of the coolant air

ρ_m - density of freestream gas

U_c – velocity of coolant air

U_m- Vlocity of mainstream gas

$\bar{u}'$, $\bar{v}'$, $\bar{w}'$ – average of fluctuating component of velocity in x, y, z direction respectively

η – Adiabatic Film Cooling Effectiveness

h_f - Heat Transfer Coefficient of the coolant film

q – Heat flux to the vane from freestream gas

T_{aw} – adiabatic wall temperature

T_w - wall temperature

T_c – coolant air temperature

T_m - main stream gas temperature

d – Coolant hole diameter

l- Length of the cooling holes

c – Chord of the blade

s – Pitch of the cascade

h – height of the blade

Ma - Mach number at inlet

Re - Reynolds number

Tu - Turbulence intensity at the inlet

M - $\rho_c u_c / \rho_m u_m$

β – compound angle of the hole

α – injection angle of the hole with reference to the mainstream gas

β_{forw}, β_{lat} – forward and lateral injection angle of the fan shaped hole

CHAPTER: 1

INTRODUCTION

1.1 Background: -

India is a rapidly developing economy, with a need for dependable and reliable supply of electricity and to be a power sufficient country is one of its prime concerns. The present installed capacity of electricity in India is 132,110.21 MW which gives the per capita consumption of power in 2005-06 as calculated by the Central Electricity Authority about 631 Kilowatt Hours. While the per capita consumption of power in developed countries like U.S is 13338 KWH. The National Electricity Policy envisages that the per capita availability of electricity will be increased to over 1000 units by 2012. So large number of new power projects are currently in progress. Thermal power plants accounts for 64.7% of the installed capacity. Because of higher efficiency gas turbine and combined cycle power plants are becoming more and more attractive with regard to reduced fuel consumption and less emissions. Modern gas turbine engines tend to push up the working gas temperature to further increase the cycle efficiency.

1.2 Motivation: -

The steady increase in turbine inlet temperature (TIT) over the last several decades has significantly enhanced the efficiency and performance of gas turbine engines. The tendency for higher turbine inlet temperature is continuing and posing considerable challenges for the analysis and design of turbine cooling schemes. The use of film cooling on the turbine airfoils helps to keep the blade metal temperature within operational limits at the cost of increased aerodynamic losses. If these losses are not minimized, it may lead to a negative increase in thermal efficiency. Hence, there is a

dire need to optimize the film cooling hole design by accurately predicting the flow physics. In this context, CFD has become a powerful tool to design and optimize film-cooled high-temperature turbine blades.

1.3 Problem Statement: -

The primary objective of this project is to computationally investigate the film cooling flow phenomenon of the first stage turbine cascade, since it is the one region which is highly thermally loaded. Geometric modeling of the two-dimension turbine cascade consisting of one blade, and a pressure and a suction side and two flow passage has been done in CFD software Gambit 2.0.1. The blade was modeled with two different types of film cooling hole viz. simple cylindrical and fan-shaped. The model was then meshed and exported to Fluent^{TM} 6.0.1solver. It was then analyzed for different blowing ratio, turbulence intensity of the mainstream gas and turbine inlet temperature.

1.4 Organization of the Report: -

An overview of the related literature has been given in Chapter 2. Description of modeling domain, governing equations used, selection of turbulence model, boundary and operating conditions applied on the cascade have been described in Chapter 3. Results followed by discussions are presented in Chapter 4. Conclusions and scope for future work is presented in Chapter 5. References are presented after Chapter 5, followed by appendices.

CHAPTER 2:

LITERATURE REVIEW

2.1 Gas Turbine: -

Of the various means of producing either thrust or power, the gas turbine engine is one of the most satisfactory. Its main advantages are: exceptional reliability, high thrust-to-weight ratio, and relative freedom of vibration. A gas-turbine engine consists of the following main parts: an inlet, a compressor, a combustor, a turbine and an exhaust, as shown in Fig. 2.1.

Nowadays there is a dire need to increase the performance of power plants and jet engines because of dwindling non-renewable sources of energy and to cut the green house gases (GHGs) emissions (the power companies has the largest share, about 60%, of the GHGs emissions). In general, speaking broadly, the efficiency of a gas turbine depends on two main factors: (i) the basic cycle efficiency of the installation, and (ii) the efficiency of the individual units. Still speaking broadly, it is said that first one is inherent in design and is not subject to deterioration in any way, whereas the second factor will vary in accordance with the condition of the equipment and the amount of maintenance given to it.

2.2 Effect of High Gas Temperature: -

The effect of the turbine inlet temperature under different loads on the thermal efficiency, SFC and net work output can be calculated using basic cycle equations and thermodynamic properties [20].

From fig. 2.2, it can be noticed that higher turbine inlet temperatures increase the net work output. Also the net work output is greatest at the higher values of the turbine's inlet temperature. With the increase of the turbine inlet temperature, the thermal efficiency will be increased while the SFC is decreased (fig. 2.3) due to a decrease in air rate. Also, it should be noted that the optimum pressure ratio for maximum effciency increases as turbine inlet temperature is increased.

2.3 Need of Cooling: -

To obtain a complete balanced picture of the safety of high temperature operation the following facts should be borne in mind: -

(i) **Failure of turbine blades** under stress at these high temperatures usually takes the form of “creep” which is a slow stretch or yield of the metal in the direction of stress. The stretch is so gradual that it can be better described as growth rather than yield. The result of creep is a reduction in blade tip clearance which, if allowed to proceed too far over too many hundreds of hours of operation, may cause a blade strip.

(ii) **The stresses in the nozzle guide vanes** are small , but at high temperatures and with sharp variation of load, as in aircraft gas turbine, the cyclic thermal stresses can and do lead to either buckling of the vane or cracking of the metal. Provided the material is sufficiently creep resistant, the later disadvantage is more likely to occur than the normal creep failure.

(iii) **The most highly stressed** portions of the turbine are the moving blades, mounted in the rotor drum or disc. Besides thermal stresses centrifugal tensile stresses, gas bending stresses and a certain degree of fluctuating bending and torsional stresses have to be carried. As the expansion proceeds through the stages of the turbine, the temperature of the gas decreases. The blade length, however, increases, and with it the centrifugal stress, but in general the conditions are less severe, and it is common practice to see highly alloyed steel in the first stage of the turbine and low alloy steel in the latter stages. In the case of the industrial gas turbine the limiting factor from the temperature point of view is not the blades but the rotor. The difficulty with the rotor is that, because of its size, it cannot conveniently be made of the most advanced materials and the highest rotor stresses tend to occur shortly after starting-up or after change of load when stresses are produced by the periphery of the rotor varying in temperature more rapidly than its bore. From this point of view the high temperature materials have the two unfortunate disadvantages of being relatively poor conductors of heat and having a relatively high coefficient of thermal expansion.

Since it is the temperature of turbine parts themselves, and not the temperature of the gas, which is the criterion of turbine conditions, it follows that, if suitable **turbine cooling** arrangements are provided, then the temperature may with perfect safety be carried far above the limit appropriate to an uncooled machine.

2.4 Metallurgical Aspects of High Temperature Gas Turbine: -

The use of high gas temperature at the turbine entry is intimately linked with the materials that can be used in such applications. The following properties are required in high temperature materials employed in gas turbines:

High strength at the maximum possible temperature,

1. Low creep rate,
2. Resistance to corrosion and oxidation,
3. Resistance to fatigue, and
4. Ease in manufacture, i.e. machinability, castability, weldability, etc.
5. At high gas temperatures, gas turbine blades work in an atmosphere that is both corrosive and oxidizing. So, for temperatures between 650^{o} C and 950^{o} C nickel and chromium based alloys are used. They have high strength and low creep combined with ductility. Cobalt alloys have high strength and resistance to oxidation up to temperatures of 1150^{o} C.

Fig. 2.4 shows the development of creep in gas turbine blades.

2.5 Various Cooling Techniques: -

The turbine blades are exposed to a continuous flow of gas that may enter the turbine at a temperature between 850^{o}C to 1700^{o}C as shown in fig. 2.5.

Modern turbine stage inlet temperatures exceed the melting point of turbine blade materials. The HPT (High Pressure Turbine) first stage blade is one component that is extremely vulnerable to high temperature. This temperature is far beyond the melting point of current materials technology. The turbine blades are required to perform and survive long operating periods at temperatures above their melting point. Various internal and external cooling techniques are employed to bring down the temperature of the blade material temperature below its melting point. Figure 2.6 shows the common cooling technique with three major internal cooling zones in a turbine blade.

The leading edge is cooled by jet impingement, the trailing edge is cooled by pin-fins, and the middle portion is cooled by serpentine rib-roughened coolant passages. Several researchers have combined these heat transfer enhancement techniques to improve the heat transfer coefficient. The cooling of the blade trailing is more challenging as it is designed as thin as possible from the aerodynamic point of view. For a thermally highly loaded blades and vanes, generally a combination of film cooling and internal convective cooling is utilized to guarantee wall temperatures within the limits of the blade material. However, it is not always recommended to combine more than one heat transfer augmentation technique.

As the cooling of the casing, nozzles, rotor blades and discs are inevitable for high temperature operation; it can be achieved either by: -

2.5.1 Liquid Cooling: -

Liquid (steam) cooling, which application is sought mainly in combined cycle power plant, appears to be more attractive on account of higher specific heat and possibility of evaporative cooling. Since heavy duty gas turbines technology partially depends on aeronautical turbines production, for a long time steam was not seriously taken into account as a coolant. In 1995, however, General Electric announced the introduction of closed-loop steam cooling in their heavy industrial gas turbine designed for combined cycle operation. Both rotor and nozzle blades are steam cooled using the steam extracted from the steam turbine at high pressure as shown in fig. 2.7. This steam is then returned at a lower pressure to the steam turbine, contributing to the power output and being contained in the steam circuit.

The approach is suitable for use in combined cycle power plants, where steam is readily available, but requires the use of sophisticated sealing technology to prevent loss of steam; the losses due to bleeding high pressure air from the compressor in an air-cooled turbine are eliminated. Other drawbacks of liquid cooling are corrosion, scale formation and choking. Steam cooling is at an early stage of development and attention will be focused on the simple analysis of the conventional air-cooled turbine.

2.5.2 Air Cooling: -

Cooling by air, besides other advantages, allows it to be discharged into the main flow without any problem. It can be tapped out from the compressor at a suitable point. The quantity of air required for this purpose is from 1 to 3% of the main flow entering the turbine stage. Blade metal temperatures can be reduced by about 200-300^{o} C by employing suitable blade materials (nickel-based alloys) now available; an average blade temperature of about 800^{o} C (1073 K) can be used. This permits maximum gas temperature of about 1400 K. Still higher temperatures are and can be used with nickel, chromium and cobalt base alloys.

Some methods of air cooling can be briefly discussed below: -

2.5.2.a Internal Cooling (convection cooling): **-**

This is achieved by passing air from compressor through internal cooling passages from hub towards the blade tip. The passages are distributed near the entire surface of the blade as shown in fig. 2.8. The cooling of the blades is achieved by conduction and convection. Relatively cooler air after traversing through the entire blade length in the cooling passages escapes to the main flow from the blade tips.

2.5.2.b External cooling (Film and Transpiration Cooling): -

It can be achieved in two ways. The cooling air enters the internal passages from the hub towards the tip. On its way upwards it is allowed to pass through the number of orifices inclined to the surface as shown in fig. 2.9. A series of such holes are provided at various sections of the blades along their lengths. The cooling air flowing out of these small holes forms a film over the blade surfaces. Besides cooling the blade surface it decreases the heat transfer from the hot gases to the blade metal.

The next step forward is likely to be achieved by transpiration cooling, where the cooling air is forced through a porous blade wall as shown in fig. 2.10. This method is most economical in cooling air, because not only does it remove heat from the wall uniformly, but effusive layer of air insulates the outer layer from the hot gas stream and so reduces the rate of heat transfer to the blade. The successful application awaits further development of suitable porous materials and techniques of blade manufacture.

2.6 Film cooling: -

The present work concerns mainly the theoretical and computational study of film cooling. Film cooling of gas turbine stator and rotor airfoil surfaces, hub and casing endwalls has played a crucial role in maintaining the structural integrity of these hot-section components at operating temperatures in excess of the melting temperature of the alloys used.

The term film-cooling refers to the use of relatively cool air extracted from the latter stages of the high-pressure compressor, which is channeled to the turbine section and is ejected into the hot flowpath through small holes in the airfoil and endwalls surfaces as shown in fig. 2.11. Ideally, this coolant air remains close to the surface to be

protected and spreads quickly between the holes to form a thin film of cool air, which isolates the component from the hot combustion gases. However, the complex flow structures present at the coolant injection site often lead to lift-off or quick dilution and therefore little protection. Higher performance demand of future gas turbine designs is leading to a need for a more thorough understanding of film-cooling behavior, better databases of film-cooling performance, and truly predictive design tools. Film-cooling designs leading to increased overall effectiveness with reduced cooling air can then be implemented with more certainty.

The same type of cooling is applied to the platforms, along the tip (shroud) and root (hub) of the vane. Internally the vanes are cooled using convection and impingement techniques. The compressed air is guided through ducts which cools the vane-material by means of convection/conduction from the inside.

2.7 Losses Incurred in Cooling: -

The increased temperature levels must be achieved with a minimum use of coolant due to the resulting engine cyclic penalties associated with the extraction of costly high-pressure air from the engine compressor stages for use as coolant. So there are two distinct aspects of cooled turbine design. First, there is the problem of choosing an aerodynamic design which requires the least amount of cooling air for a given cooling performance. The second aspect is the effect on the cycle efficiency of losses incurred by the cooling process; a pertinent question whether it is advantageous overall to sacrifice some aerodynamic to reduce such losses. The sources of losses are as follows: -

1. There is direct loss of turbine work due to the reduction in turbine mass flow.

2. The expansion is no longer adiabatic; and furthermore there is negative reheat effect in multi-stage turbines.
3. There is a pressure loss, and a reduction in enthalpy, due to the mixing of spent cooling air with the main gas stream at the blade tips. (This has been found to be partially offset by a reduction in the normal tip leakage loss).
4. Some pumping work is done by the blade on the cooling air as it passes radially outwards through cooling the passages.
5. When considering cooled turbine for cycle with heat exchange, account must be taken of the reduced temperature of the gas leaving the heat exchanger less effective.

Cycle calculations have shown that even when all these losses are accounted for, there is a substantial advantage to be gained from using a cooled turbine.

2.8 Theoretical background: -

Because of its crucial role in preventing thermal failure, for the last three decades, film cooling in gas turbine vane has became an extensive area of research both experimentally and computationally which has revolutionised the film cooling design. The studies include injection through a single hole and multiple hole arrangements, as well as the effects of geometry (e.g., hole angles hole length and spacing). Many studies, in order to simplify the geometry, have modeled the airfoils as flat plates or cylinders with discrete cylindrical hole film cooling schemes. But with the advancement in technology, the effect of curvature has been shown by many authors. The motivation behind every film cooling investigation is to minimize the coolant flow by studying number of simplified geometries and working conditions.

2.8.1 Film Cooling Parameters: -

Film-cooling has been one of the most extensively studied cooling methods over the last two decades due to its wide variety of practical applications in high-temperature systems such as turbine blades, end walls, combustors, and after-burners. A lot of studies have been performed to enhance film-cooling effectiveness for various injection systems in case of turbine vane. Designers are trying to achieve greater cooling performance from less coolant air, particularly in next-generation high-efficiency gas turbines. To make significant advances in cooling technology, it requires a fundamental understanding of the physical mechanisms involved in film-cooling flow fields. Definition of coordinates and dimensions of the cooling hole are given in fig. 2.12.The film cooling performance is influenced by variety of parameters which can be listed as below:-

i. Hole geometry viz. hole shape (cylindrical, fan shaped), length to diameter ratio

of the hole (l/d), injection angle, compound angle.

ii. Blowing ratio (M): - This is one of the most important parameter which has an impact on flow physics. It is defined as $\rho_c U_c/\rho_\infty U_\infty$.

iii. Incoming Mainstream Turbulence Intensity = $\sqrt{1/3(\ \overline{u}'^2 + \overline{v}'^2 + \overline{w}'^2)}/u_{mean}$

iv. Density ratio (DR) and Momentum Flux Ratio (IR): - $DR= \rho_c/ \rho_\infty$, $IR=DR^2/M$

v. Heat Transfer Coefficient, h_f and Adiabatic Film Cooling Effectiveness, η : -

In contrast to two-temperature heat transfer problems, film cooling is dominated by three temperatures: the temperature of the hot gas, the temperature of

the injected cooling film, and the resulting wall temperature. The heat transfer to a film-cooled surface is commonly described by: -

$$q = h_f \, (T_{aw} - T_w)$$

where the adiabatic wall temperature T_{aw} is a reference temperature and T_w is the vane wall temperature. T_{aw} is presented in terms of non-dimensional film cooling effectiveness η given by

$$\eta = (T_{aw} - T_\infty) / (T_c - T_\infty)$$

Thus, the film-cooling effectiveness describes the cooling potential of the injected film without any heat flux into the wall. The heat transfer coefficient, h_f, considers the influence of the coolant injection on the heat transfer process due to the modified fluid dynamics. It does not depend on the temperature boundary layer condition. Both of these two parameters have to be known to calculate the wall heat flux accurately.

2.8.2 Review of the types of holes: -

On the basis of the shape, orientation and geometry different kinds of cooling holes have been discussed with the sole aim to either reduce the coolant supply or to improve the film cooling performances. Sometimes cost constraint is also considered. All types are discussed herein: -

2.8.2.a. Simple Cylindrical Holes with Normal or Inclined Injection: -

Originally cooling holes were developed in cylindrical shape and used even nowadays because of their ease of manufacture. As the normal injection leads to heavy mixing with the cross flow leading to decreased cooling effectiveness, there are not in

use now. A simple cylindrical hole is shown in fig.2.13. Note that the injection angle, α, is the angle between the hole axis and the plane tangent to the vane surface at the point of coolant injection. Injection angle, α, varies normally between 30^o – 60^o.

2.8.2.b. Cylindrical Holes Having a Compound Angle (β): -

Compound angle is implemented in modern designs to improve the lateral spreading of the coolant and therefore provide more uniform coverage. However, in past studies it was found that compound angle also leads to undesirable increases in surface heat fluxes. In order to use this coolant geometry effectively, the mechanisms responsible for the contradictory surface results for adiabatic effectiveness (h) and heat transfer coefficient (h) must be fully understood so that compound angle injection can be effectively implemented in future designs with greater confidence. Compound angle (β) is measured in x-y plane in the clockwise direction. β is normally given a value of 45^o-90^o (a value of 90^o is generally given in case of showerhead cooling).

2.8.2.c. Fan Shaped Holes: -

In these type of holes, a forward or lateral or both expansion at the hole exit is provided for better cooling performance.

By expanding the exit of the cooling hole in the lateral direction, the effective momentum of the surface coolant can be reduced prior to injection. Fan-shaped holes provide better surface attachment at higher blowing ratios, as well as better lateral spreading of the coolant than cylindrical holes. The major drawback for non-cylindrical hole geometries is increased initial manufacturing costs. The benefits, however, of fan shaped holes are many, including increased part life (fewer replacements needed), less required coolant (increased engine efficiency), and fewer holes needed (increased

structural stability of the vane). The forward and lateral diffusion angle β_{forw} and β_{lat} (as shown in fig. 2.14) is generally given a value between $10^o - 20^o$.

2.9 Summary of Past Studies: -

Goldstien *et al* [20, 21] provided an early review of these film cooling techniques and measured experimentally the film cooling effectiveness and heat transfer coefficient distribution on inside hole surfaces, internal walls and on the exposed surface for a blowing ratio of 0.2 to 2.2. Actually he used heat/mass transfer analogy to convert mass transfer results into heat transfer results to avoid any error (it is very difficult to measure the heat transfer rate inside the holes as such measurement involves large conduction error due to variation in heat transfer rate resulting from sharp temperature gradients at the hole entrance.) He showed that Sherwood no. is high on the side of the hole due to the interaction of the coolant with the mainstream gas. The mass transfer around the hole was dominated by the formation of horse shoe, side and kidney vortices generated by jet stream and cross flow interaction as shown in fig. 2.15. The film cooling effectiveness was high and uniform in the streamwise direction but not in the lateral direction.

In order to improve the lateral distribution of coolant, studies were focused more on the double row of cylindrical holes. Abhari *et al*. [4] results showed that for the same injected mass flow rate per unit span the double row arrangement provides better cooling effectiveness compared to injection from a single row. Staggered rows show better performance than rows with inline arrangement. The gain in effectiveness was due to the lower penetration of the coolant jets because of lower momentum ratio resulting from the increased injection area and better lateral spreading of the cooling air.

Increasing the distance between the two rows give a significant decrease to both local and lateral averaged effectiveness, especially close behind the downstream row. A compound angle orientation of the holes, especially of the second row, increases cooling effectiveness. Recent studies on film-cooling holes with a diffuser-shaped expansion at the exit portion of the hole ‘‘so called fan-shaped’’ have shown a promising improvement of the film cooling performance.

Various research groups Gritsch *et al* [12] and Colban [12] investigated film-cooling effectiveness with injection from different hole shapes, including holes with a lateral or forward expanded exit part. They all found higher effectiveness values for the shaped holes compared to cylindrical holes with the same arrangement. The fan shaped hole performed better because its reduced jet momentum allowed the jet to stay attached to the surface and spread out and cover a larger surface area. Due to the reduced jet exit momentum, shaped holes show less penetration of the coolant jet into the mainstream and reduced velocity gradients in the mixing. But the increased manufacturing cost has to be done when using shaped hole geometry.

Colban *et al* and Haendler [9], presented a detailed experimental and computational investigation of film cooling on a gas turbine vane with fan-shaped holes. Multirow data were presented at a range of engine representative blowing ratios on both the pressure and suction sides and compared to CFD predictions using both the RNG k- ϵ and v^2-**f** turbulence models. He reported that showerhead blowing on the pressure as well as suction side was not so effective due to jet lift-off leading to little cooling in that region. The first pressure side fan-shaped row exhibited liftoff and reattachment, as evidenced by a narrowing and widening in jet contours, although the

liftoff was not as significant as the single-row case. Overall, film cooling effectiveness levels increased on the pressure side with both surface distance and blowing ratio. The CFD predictions did not agree well with the experimental results either capturing the correct effectiveness levels or the correct physics, but not both. The v^2-**f** model more nearly predicted the actual flow physics, whereas the RNG k- ϵ model offered a better match with the experimental data in terms of correct effectiveness levels. Although there have been matching CFD predictions for flat-plate film cooling, clearly more advances in CFD turbulence modeling are required before the highly complex flow of film cooling on a gas turbine vane can be modeled accurately.

Waye and Bogard [5] compared the effectiveness of axial and compound angle holes on the suction side of the turbine vane. The effect of the surface curvature was also evaluated by comparing to previous curvature studies and flat plate film cooling results. Results showed that for mild curvature, flat plate results are sufficient to predict the cooling effectiveness. Furthermore, the compound angle injection improves adiabatic effectiveness for higher blowing ratios, similar to previous studies using flat plate facilities. Also effectiveness levels were higher for high mainstream turbulence at moderate and high blowing ratio. It can be attributed to increased mixing with the mainstream, which brought some of the coolant back to the surface. Also, as expected, effectiveness values were higher for smaller hole pitch since there was more coolant mass along equal lateral distance. In fact, the values were two times the values of the larger pitch.

Although film holes with non-cylindrical exit shape have received increasing attention during the last years, there are only very few studies that try to find out which

are the governing geometrical parameters that really affect the thermal performance of the hole. Most of the studies focused on a comparison of fan-shaped hole performance versus a standard cylindrical cooling hole.

Gritsch *et al*., Thole et al [19] compared the performance of two different fan-shaped holes in terms of film-cooling effectiveness and heat transfer coefficients. They found that the thermal performance of a hole that diffuses in both lateral and streamwise direction (laidback fan-shaped hole) is superior to a hole that only diffuses in lateral direction, in particular at high blowing ratios. The area ratio of both holes were almost identical (AR=3.0) for the lateral diffusing hole and AR=3.1 laidback fan-shaped hole. Saumweber *et al*. [10] investigated a row of holes that had identical shapes as those of Gritsch *et al.* at elevated turbulence levels. They found that the fan-shaped and the laidback fan-shaped hole performances were very close. The same type of hole shapes have also been investigated for leading edge cooling applications .The performance of the laidback fanshaped hole was found to be superior to the fan-shaped hole for this case.

Kohli and Bogard [18] compared two fan-shaped holes featuring the same lateral diffusion angle but different forward diffusion angles of 15 and 25 deg. The hole with the larger forward diffusion angle was expected to keep the coolant jet closer to the surface. However thermal performance of this hole in terms of film cooling effectiveness was found to be lower than for the hole with the smaller forward diffusion angle due to flow separation in the diffuser part of the hole.

Table 2.1: A brief of the recent investigations on film cooling.

Author	Hole type; Arrange-ment	Pit-ch (P/D)	Inject ion Angle (α)	Blowing Ratio (M)	Solver and Model selected	Remarks
Bernsdorf, Rose *et al*; 2008 [1]	Axial; staggered	4	30°, 50°	0.99-2.69	Multi3; Burdet-film-cooling model	Quassyste-ady assumption of film cooling
Karsten Kusterer *et al*, 2007 [2]	Axial; Staggered	3	30°	1.61-1.78	CHT flow; Baldwin–Lomax algebraic eddy–viscosity	Film effectiven-ss investigate-on
Waye, Bo-Gard, 2007 [5]	Axial; staggered	2.8	30°	0.3-1.4	Experimental only	Film effectivene ss
Yoji Okita, Masakazu Nishiura,2-007 [3]	Arrowhead, Fanshaped; Staggered	4.4	35°	0.6-3.5	Fluent 6.0.1; Standard κ-ω model	Comparis-on of effective-ess on ASH, FSH
Andre Burdet; Reza S. Abhari; 2007 [4]	Cylindrical, Fan-shaped	4	30°, 60°	1,1.5	Multi3; Burdet-film-cooling model	Feature based jet model reduced computati-onal overhead
W. Colban, K. A. Thole, M. Haendler	Fan-shaped; Inline	4	60°, 30°		Fluent 6.0.1; RNG k-ε. V^2f	Significant showerhe-ad lift-off; RNG k-ε agreed better with the experiment.
Rutledge, Robertson; 2006 [8]	Axial, Staggered	4	25°, 56°	0.3-1.4	Experimental only	Effect of roughness on effectiven-ess

P. Martini A. Schulz H. J. Bauer [10]	Pin-fins at the trailing edge	----	----	----	Fluent 6.1; Direct Eddy Simulation (DES)	Simulation of trailing edge film-cooling
Gritsch *et al*, 2005 [12]	Fanshaped, Compound angle	4-6	30^o, 60^o	0.5-2.5	Experimental only	Effect of hole geometry on thermal performan-ce
Dittmar *et al*; 2003 [14]	Axial, shaped, compound angle	4	45^o	0.5-3.0	Experimental only	Assessme-nt of different film cooling Configurati-ons

2.10 Figures: -

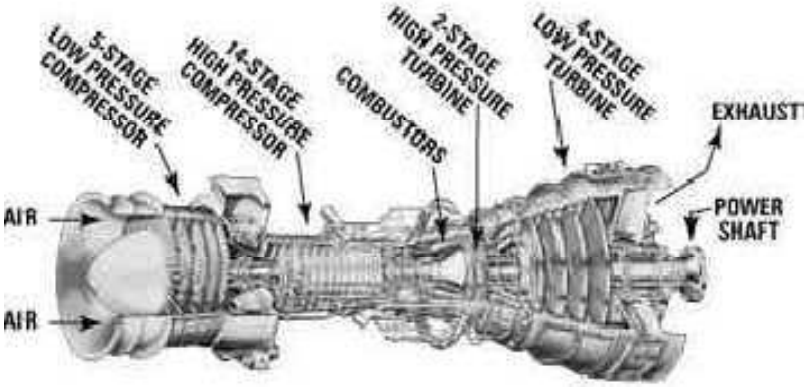

Fig.2.1: A schematic representation of a gas turbine [31]

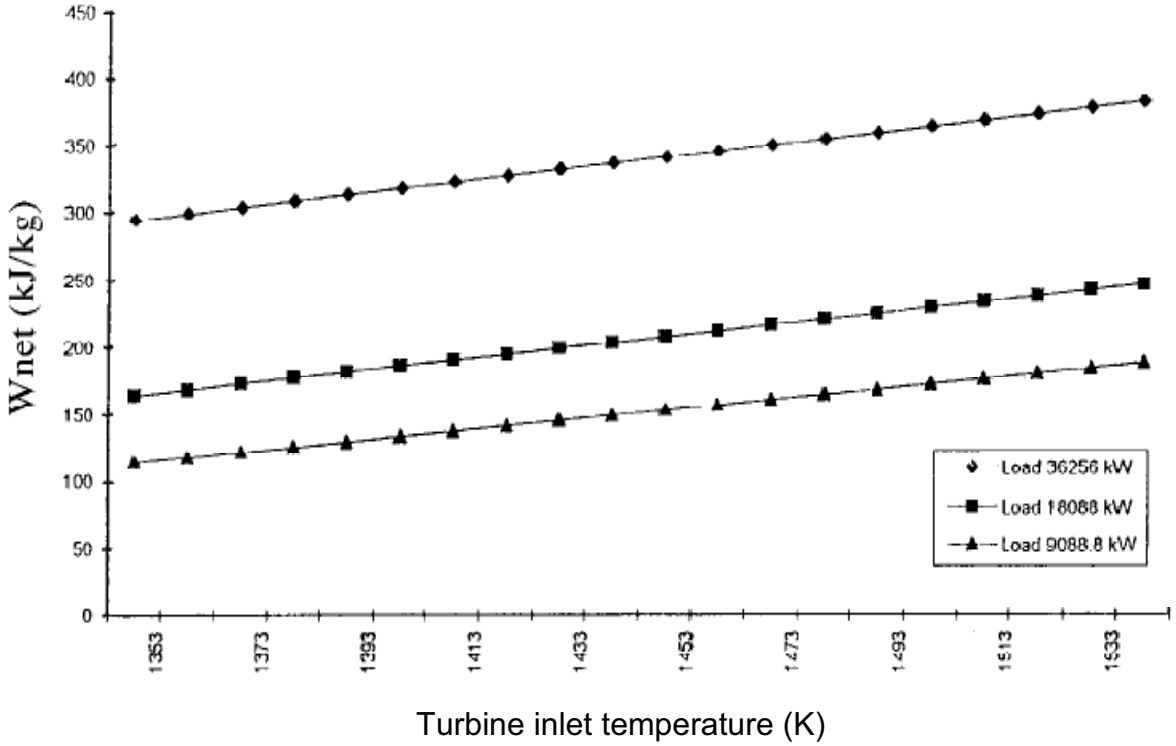

Fig. 2.2: Effect of turbine inlet temperature net work output. [26]

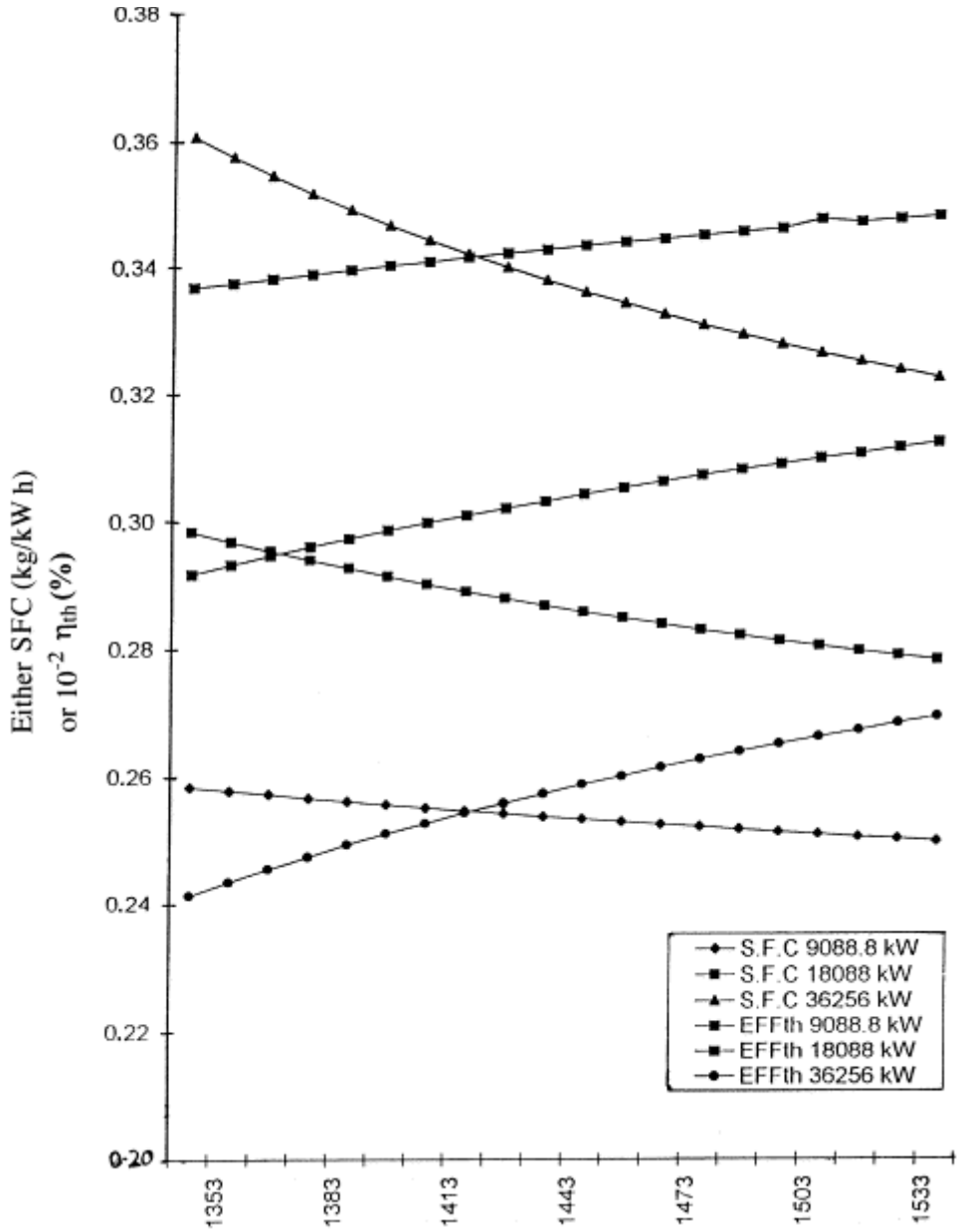

Fig. 2.3: Effect of Turbine inlet temperature on thermal efficiency and specific fuel consumption. [26]

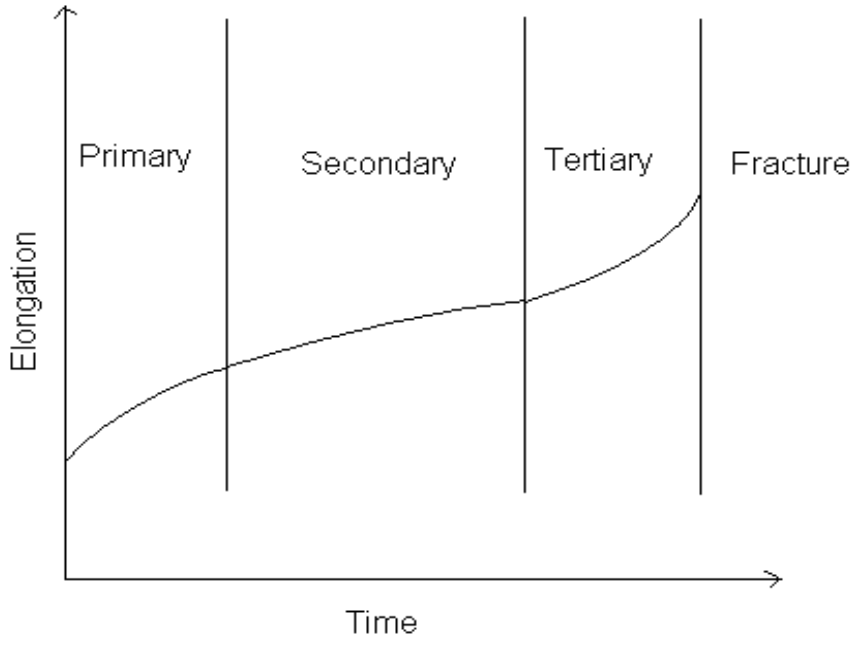

Fig. 2.4: Creep in gas turbine blade.

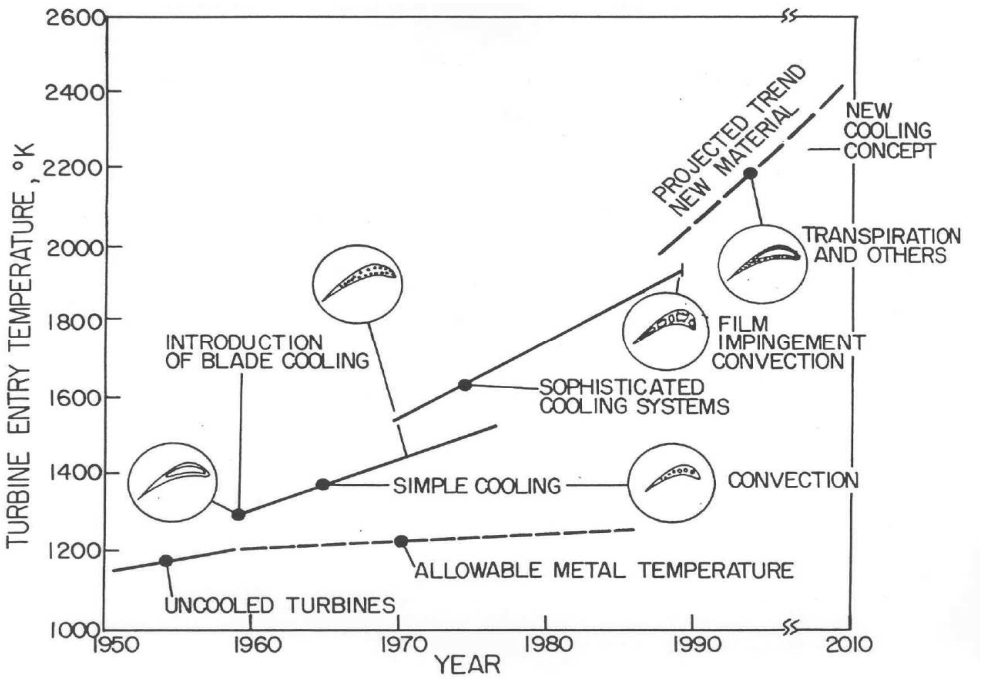

Fig.2.5: Cooling trend [21]

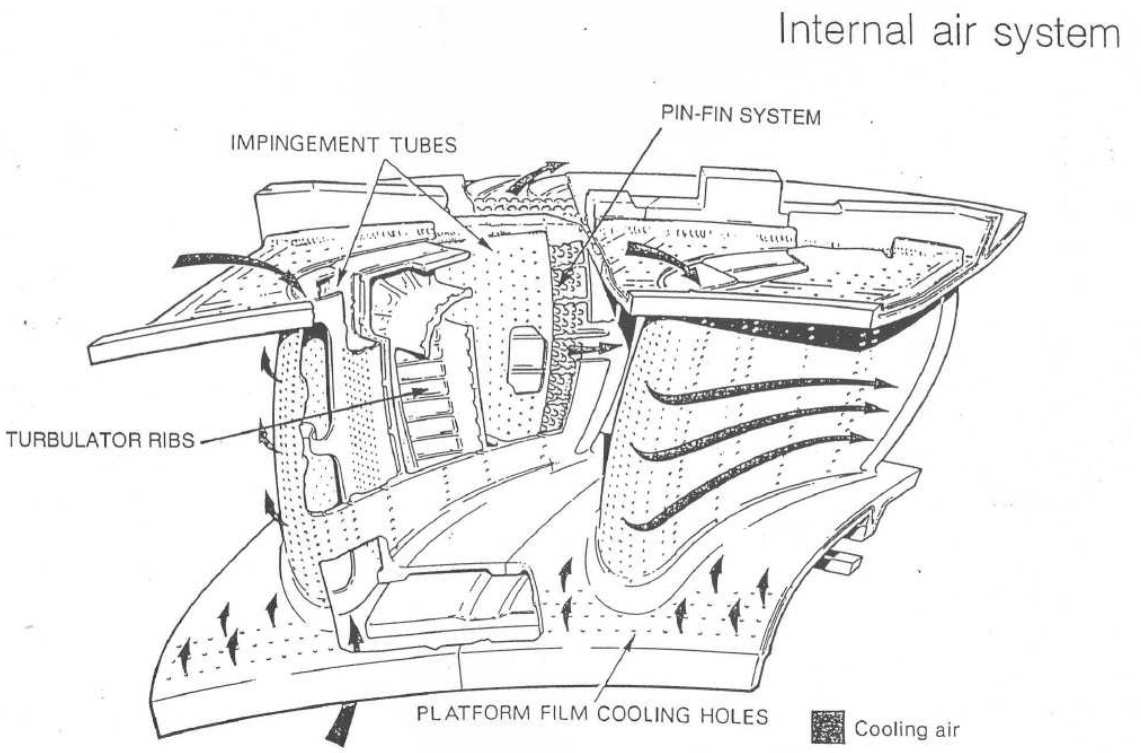

Fig. 2.6: Cooling schemes for Inlet Guide Vane. [22]

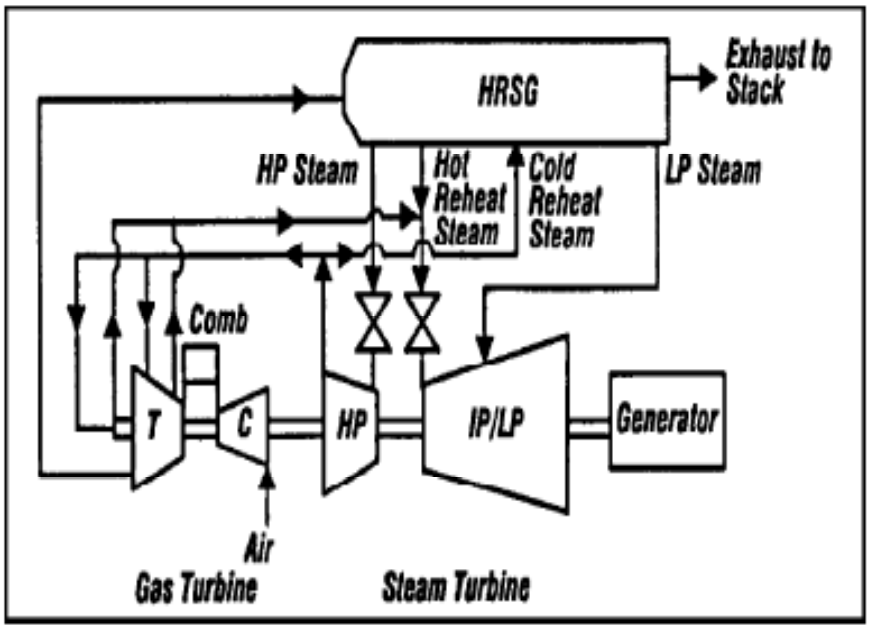

Fig. 2.7: Approximate scheme of a combined plant with gas turbine cooled with steam in closed loop.

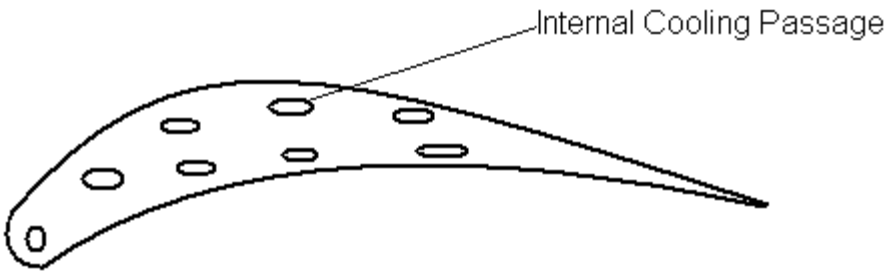

Fig.2.8: Convection cooling.

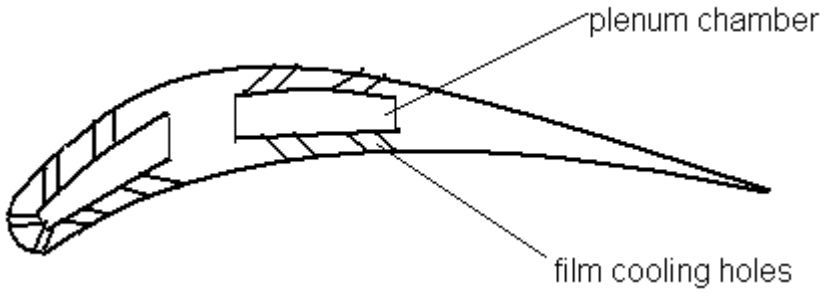

Fig. 2.9: Film cooling.

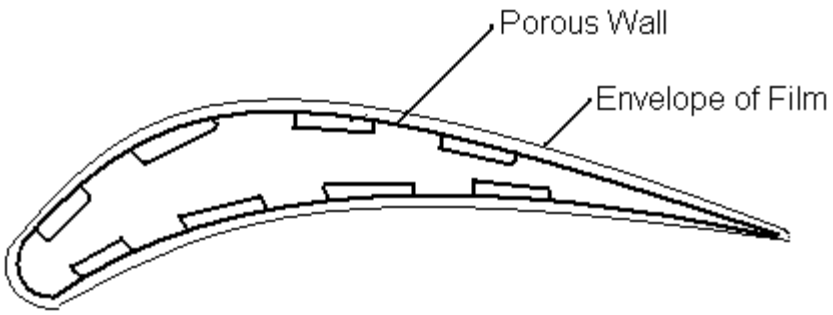

Fig. 2.10: Transpiration cooling.

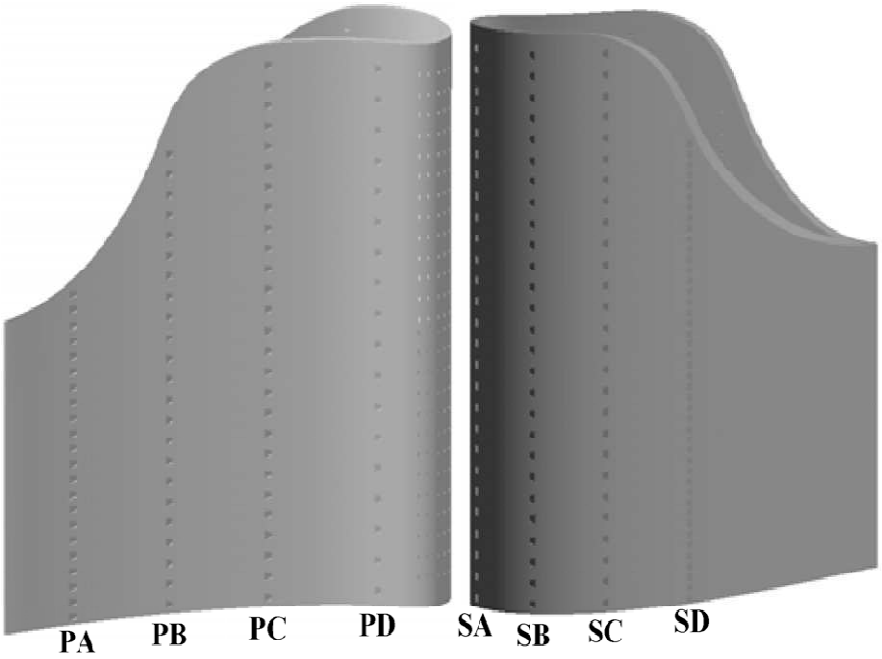

(a)

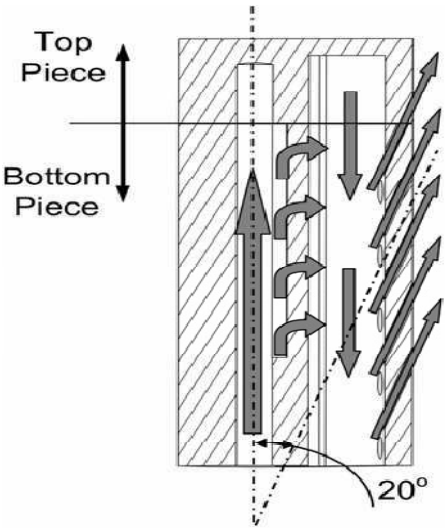

(b)

Fig.2.11: Turbine vane showing film cooling holes on the pressure and suction side (a) and flow of coolant inside the hole (b). [9]

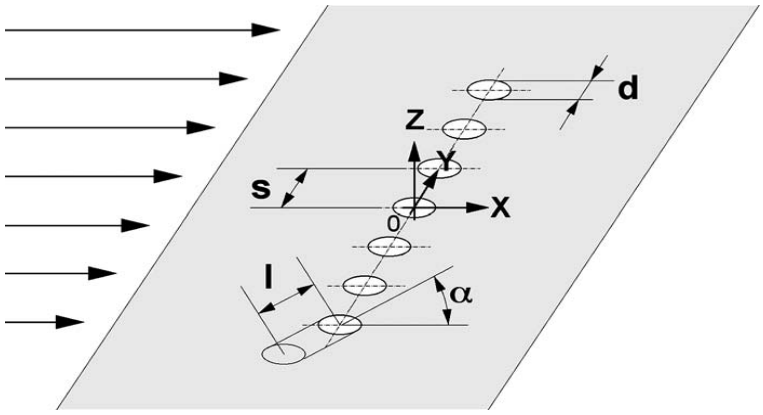

Fig 2.12: Main geometrical parameters of the cooling hole. [1]

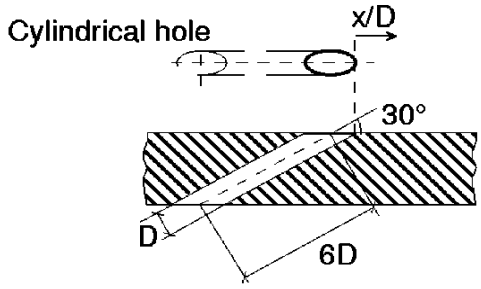

Fig 2.13: A Simple cylindrical hole.

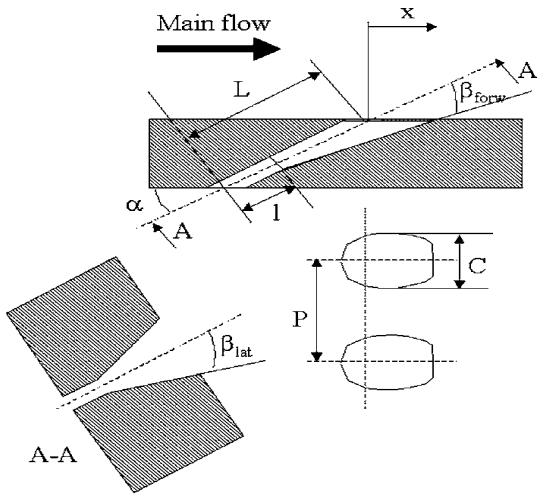

Fig 2.14: A Fan Shaped-Hole with lateral and forward diffusion. [12]

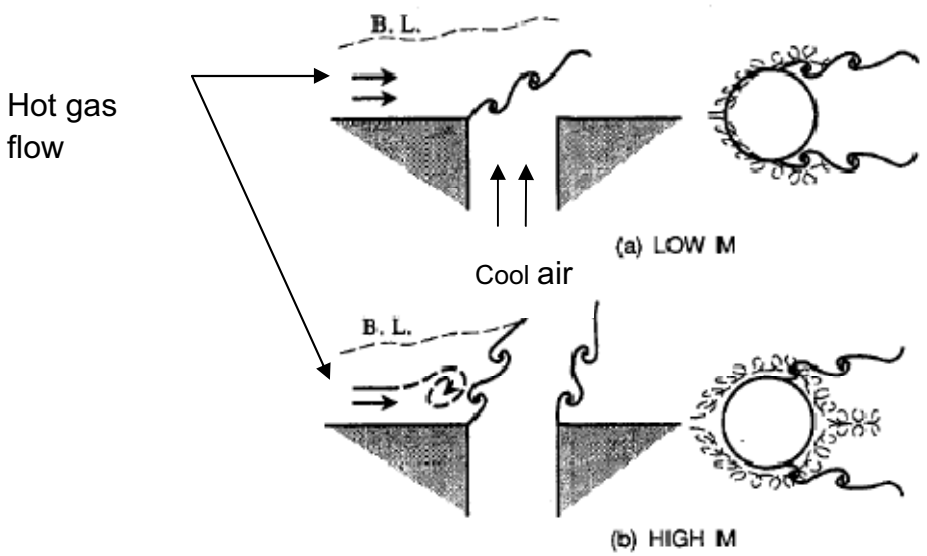

Fig. 2.15: Interaction of mainstream gas with coolant jet (M = Blowing ratio). [16]

CHAPTER 3

MODELING OF FILM COOLING AND COMPUTATIONAL METHODOLOGY

3.1 Prerequisites of the Modeling of turbomachinery flow field: -

The object of this work is first to predict computationally, using commercially available software FLUENT^{TM} 6.0.1code, the temperature distribution and flow structure of an un-cooled turbine vane cascade and then their comparison with the film cooled turbine blade with simple cylindrical holes and fan shaped holes.

Modeling of the flow physics for turbomachinery components encompasses the selection of a representative set of governing equations, the assignment of appropriate boundary conditions, and, for the case of turbulent viscous flow, the choice of a turbulence model. The degree to which a CFD code functions successfully depends upon how closely it meets certain requirements.

Representation of the geometric configuration of the component, via the solution grid, must reflect physical reality. Solution grids or mesh must be able to accurately depict blade and flow path shapes, and model complex details such as film cooling holes, as in this work. In addition, these grids must be able to resolve the details of flow structure. The proper selection of a solution grid is essential to ensure the accuracy of both the modeled component geometry and the flow analysis.

The specification of boundary conditions for the governing equation should be general enough to accommodate all types of boundaries encountered in turbomachinery flow paths. In addition, the selection of a turbulence model should adequately account for the characteristics of typical turbomachinery flow fields, such as flow path curvature, rotating flow, high pressure gradients, and separated, recirculating flows.

The selection of numerical techniques is also a critical issue. Discretization of the governing equations and choice of the solution technique for the resulting finite-difference or finite-volume approximations to those equations must be properly done. Finally, post-processing must be given due consideration to interpret the results of a completed analysis.

3.2 Three-Dimensional Geometric Modeling: -

Most of the recent works have been done in three dimensions which model and capture well the flow structures of film cooling flow particularly the well known counter rotating vortices (CVP). In this work, initially a 3-d cascade of the first stage turbine nozzle guide vane was modeled with film cooling holes and plenum chambers. The geometric modeling of the 3-d cascade with film cooling holes and plenum chambers was little demanding as it requires a good expertise of solid modeling. The generation of the 3-d model is explained in the following steps: -

(1) The vertex data of 6030 blade profile was first imported into Gambit 2.0.2. The vertices were then joined to form edges which were eventually transformed into the face of the blade.
(2) Plenum faces, two in this case, were then generated by creating points on the face of the blade and then joining them. The shape of the plenum was chosen from the available literature[ ].
(3) Blade face was then swept in the positive z-direction to a length of 100 mm to form three dimensional cascade.
(4) Similarly, plenum faces were swept to a length of 90 mm to represent the plenum volume.

(5) After that, plenum volumes were separated from the blade volume by subtracting them from the later. While doing so, the retain option in Gambit was checked for the plenum volumes as they (plena) represent the coolant air inside the blade.

(6) The last step was the creation of film cooling holes projecting from the plena to the pressure and suction surface of the blade. Two solid cylinders of diameter (d = 1 mm) and length (l = 3 - 6d), with axis lying on the x-y plane, and oriented at 30^0 - 60^0 with the streamwise direction, were defined on the suction and pressure sides. The cylinders were then copied (number of copies = 13) on each side of the blade having a pitch of, p = 5mm, to form the first row of cooling hole.

(7) In a similar fashion, the other four rows, with staggered arrangement, were created. Total number of cooling holes was 70 on each side. Since the cooling holes and plenum chambers are the same entity representing the coolant air flow, so their volumes were united subsequently.

` The plenum chambers and film cooling holes is shown in the solid model and the wireframe model in fig. 3.1 and 3.2.

The model also included two flow channels, extended inlet and outlet regions, and the end walls. When the domain including the holes and the feeding plena were meshed with unstructured tetrahedral cells, it led to an unacceptable number of grid nodes (around 2.75 million). A similar number of grid nodes (2.2 million) appeared in a CFD prediction done by W. Colban *et. al.*, 2007 and M. Haendler, 2007**,** in Fluent 6.0.1 with RNG κ-ε turbulence model. Its convergence required ~1000 iterations on four parallel processors. The simulation took approximately two days to converge. In the present work the available resources are Pentium^{TM} 3.2GHz processor and 2GB

Physical memory, so it was hardly feasible to solve the full 3D model with the available computational resources due to the requirement of very large computational time to many days for the mathematical iteration. Eventually the 3D CFD model was aborted and a 2D computational domain was modeled for the investigation of flow physics of film cooling.

3.3 Limitations of the Two Dimension Model: -

(1) It is not possible to model the jet secondary flows as shown in fig.3.3 in 2D.The jet flow behavior in the immediate vicinity of the hole exit is highly three-dimensional as shown in fig. 3.3. It contains flow features that are of primary importance for the downstream convection and diffusion of the coolant fluid with the freestream flow. Between the hole exit and the plane of injection, the coolant jet bends due to the inertial force of the freestream. The trajectory of the jet is the primary flow feature that affects the coolant fluid penetration. After flowing out of the hole, the coolant starts to mix with the freestream, on a length scale that is much smaller than the hole diameter. This lowers the penetration velocity of the coolant fluid located near the wall, allowing the freestream fluid to penetrate more easily underneath the core of the jet. The vorticity ring coming out of the hole (from the jet boundary layer) bends and squeezes, forming the well-known counterrotating pair of vortices.

(2) The absence of plenum chambers in 2D simplifies the flow structure which prevails in three dimensions as shown in fig. 3.4. There is very large flow acceleration when the coolant enters into the hole from the plenum as the area of the hole is very small relative to the plenum. Besides, there is excessive turning at the sharp-edged entrance to the film hole. At an injection angle of 35 deg, some of the coolant has to go

through a turn of 145 deg into the film hole at the downstream side of the plenum. The inability of the coolant to negotiate this turn leads to a large three dimensional separation along the downstream surface of the film hole. This separation region results in nonuniform coolant distribution, secondary motion within the film hole high-velocity gradients high turbulence generation.

3.4 Description of the Simulated Two Dimensional Domain: -

The two dimensional view of the investigated computational domain with applied boundary conditions has been shown in fig. 3.5.

It covered one blade and two flow paths. The inlet plane was placed at a distance of 0.30 of axial chord upstream of the leading edge, whereas the outlet plane was located at a distance of 0.5 axial chord downstream of the trailing edge, so as not to affect the upstream flow field. The profile of the blade was 6030 whose co-ordinates are given in Appendix 2. It is from the first stage of the HP turbine and is of the reaction type.

3.5 Preprocessing: -

3.5.1 Geometric Modeling: -

A 2-D model of the profile was created in Gambit 2.0.2, a commercially available software from Fluent 6.0.^{TM} Inc. The vertex data were imported and then joined to form edges, which were eventually merged to form suction and pressure sides of the blade. After that, these two sides were copied on the opposite sides of the blade to form the edges of the blade passage. Edges were then joined to form the blade and two passages. The domain was then extended on the either side of the leading edge and the trailing edge.

3.5.2 Modeling of Film Cooling Holes and Plenum: -

The film cooled guide vane constituted five cooling hole on suction side and five on pressure side as shown in fig. 3.6. Three circular plenum chambers were created on the blade surface which feed the cooling air, bled from the compressor, to the cooling hole. Two types of hole geometries were investigated; a simple cylindrical hole and a fan-shaped hole. Blade with fan-shaped holes is shown in fig.3.6. The pressure and suction side edges are designated as pe1 to pe6 and se1 to se6 respectively just to facilitate post-processing of the results. Their baseline geometry is shown in fig. 3.7. The complete geometry of both the types of holes is given in table 3.1. The diameter of all the cylindrical hole (actually rectangular in 2D) and fan shaped hole at the inlet is 0.5mm. The diameter of the shaped holes at the outlet depends upon the length of the hole and is given in table 3.1.

Shaped holes are given a forward expansion angle of $\beta = 10^0$. The expansion is given in two-third of the outside length of the hole. The inclination angle of both the holes at their respective positions is kept same. Entry and exit of the holes are sharp edged. The interior surfaces aerodynamically smooth. Each cooling configuration is simulated for different values of blowing ratio, turbulent intensity of incoming mainstream flow and surface roughness of the vane. During all the simulation the static temperature ratio, T_c/T_m ratio is kept constant at 0.6 leading to a density ratio of ρ_c/ρ_m=1.67. A complete set of operating conditions is given in table 3.1

Table 3.1 Cascade dimensions and flow parameter.

S. No.	Parameters	
1.	Profile	6030
2.	Cascade type	Rectilinear
3.	Type of simulated blade	Reaction type
4.	Chord (mm), c	50
5.	Pitch (mm), S	25
6.	Height (mm), h	95
7.	Blade stagger angle	80°
8.	Inlet flow angle	35°
9.	Number of blades	3
10.	Number of channels	2
11.	Working fluid	Air
12.	Total no. of cooling holes	10
13.	Total no. of plenum chambers	3
14.	Diameter of the cooling holes (mm), d	0.4 - 0.6
15.	Streamwise injection angle (α)	90^0, 60^0, 30^0
16.	Length of the cooling holes (l), mm	3-6d
17.	Shaped holes forward expansion angle, β	10^0
18.	Shaped hole outlet diameter for $\alpha = 30^0$	d + 0.338L
19.	Shaped hole outlet diameter for $\alpha = 60^0$	d + 0.151L
20.	Hole pitch to diameter ratio, p/d	3-8
21.	Inlet velocity of mainstream gas. U_m	56 m/s
22.	Inlet Velocity of the coolant, U_C	6.8, 16.4, 32.8 m/s
23.	Mach number at inlet, Ma	0.125
24.	Reynolds number based on inlet velocity of the gas, Re	95,8542

25.	Turbulence intensity at the inlet, Tu	7-20%
26.	Hot gas temperature, T_m	500 K
27.	Coolant air temperature, T_C	300 K
28.	Density ratio (constant), $\rho_c/\rho_m=T_m/T_C$	1.67
29.	Blowing ratio, M (varying), $\rho_c u_c/\rho_m u_m$	0.18, 0.5, 1.0

3.5.3 Grid Generation: -

Once the geometric model is established, the next step in the process of communicating this configuration to the CFD analysis program is to define the computational grid within the physical domain. The governing equations are solved at every point on the grid, or within every cell formed by the grid. So the grid imposed on the physical domain must provide adequate resolution in all areas of the flow field to permit adequate prediction of the flow behavior.

3.2.3.a. Types of Grid and Their Suitability: -

Depending upon the type of construction, a computational grid may be classified in two types: -

(I) Structured Grid: - A structured grid has a fixed number of points in each of three or two (for 3-d, 2-d) directions, and the grid lines are arranged according to some scheme that is related to the geometric configurations of the physical domain as shown in fig 3.9 (a). Common types of structured includes H-grids, C-grids, and O-grids. These grids are generated by using either algebraic methods, where grid coordinates are interpolated by using algebraic functions, or differential equation methods which uses

partial equations, such as Poisson's equations, to determine the positions of grid node coordinates. An example of a structured grid has been shown in fig.3.9.

(ii) *Unstructured Grid*: - Unstructured grids are not oriented in any particular direction, nor do they have a fixed number of points in any particular direction as shown in fig. 3.9 (b). These are generated by first establishing a suitable distribution of grid points on each boundary surface of the physical domain, without imposing any predetermined connectivity on the points. As unstructured grid is not sensitive to the complexity of the physical domain, they can be generated with much less effort, and in much less time, than is required for structured grid.

As the complexity of the physical domain increases, the application of the structured grid becomes more difficult, and special gridding techniques are employed. The multiblock grid generation technique allows structured to be generated more easily for complex configurations, by simplifying the definition of surface boundaries. However this is obtained at the increased computational effort.

However, some cases, for instance, an analysis of flow through complex internal cooling passages in a turbine combined with the mainstream gas flow, can render even multiblock techniques ineffective. To satisfactorily mesh such complex domain, the most effective approach is to apply an unstructured grid. Two significant advantages of the unstructured mesh capability in **FLUENT** are: -

(i) The reduced setup time compared to structured grids,

(ii) The ability to incorporate solution-adaptive refinement of the mesh.

3.5.3.b. Computational grid in the present work: -

A coolant jet in cross flow (JICF) in a turbine is a multiscale flow problem. The coolant jet gradually mixes with the free-stream at a characteristic length scale of the hole diameter (e.g., 0.5–1.0 mm). In contrast to this, the aerodynamics of the passage, e.g., passage vortex, has much larger length scales. These scales may differ by up to two orders of magnitude. Therefore, a relevant numerical simulation must be made with a mesh that allows at least the prediction of the important fluid structures of the smallest geometric scale, namely, the hole diameter.

In the present work, quad - map, a structured mesh, was applied initially but the grid check failed due to the presence of negative volume. Then quad – pave, an unstructured mesh scheme, was applied which succeeded. First the edges were meshed with even number of intervals as it is a criterion for face meshing using quad – pave scheme. Then the faces were meshed. As shown in fig. 3.10, a very fine mesh was created inside the hole and near hole region to resolve the flow structure existing there and a relatively coarse mesh away from the hole. The details of the mesh information are given in Appendix 3.

3.5.4 Boundary and Continuum Type Specifications: -

The solution of the governing equations is performed over a finite space, on which a computational grid has been imposed. In order to properly model the flow physics within this space, a set of appropriate boundary conditions is specified for the governing equation. Three different types of boundaries can be identified for the typical turbomachinery flows: -

1) Wall boundaries; 2) inlet and exit boundaries; and 3) periodic boundaries.

The most common types of inlet boundary condition are velocity inlet, mass flow inlet and pressure inlet. Wall boundaries consist of blade surfaces and edges, passage end walls. These may be rotating, non-rotating or a combination of both. For solid walls, a zero relative velocity or no-slip condition is appropriate. Further details can be taken from the referenced literature.

In the present study velocity inlet condition has been specified at the inlet of the blade passage and pressure outlet condition at the outlet. For the flow through the cooling holes again velocity inlet condition was specified. Velocity was specified by using the component and direction method in Fluent. The mainstream velocity was set at 56m/s and the temperature was set to 500 K. This yielded Mach No. of 0.125 at the inlet. Turbulence was specified by defining turbulence intensity and hydraulic diameter. At the entry turbulence was varied between 7– 20% to study its effect on the film cooling performance. Hydraulic diameter was given a value of 25 mm. Coolant air entered the hole with an ambient temperature of Tc = 300 K. The coolant flow velocity at the inlet boundary was set to values between 6 and 13 m/ s providing the correct coolant mass flux for blowing ratios M = 0.5; 0.8; 1.1. Wall conditions were imposed on the blade edges, plenum edges, cooling hole's edges and on the outer edges of the domain as shown in fig. 3.2. The data for the boundary conditions was taken from the experiments conducted by **P. Martini** *et. al*.**, 2006** and **C. F. Whitney, 2006,** at ALSTOM Power Technology Centre, UK.

In the continuum type specification, fluid type was defined for the ten hole faces and two channels faces. The blade faces were specified as solid type.

3.6. Computational Issues: -

3.6.1 Governing Equations: -

For the flows encountered in turbomachinery components, the mathematical models are always based on the famous Reynolds – averaged Navier - Stokes (RANS) equations. The set of governing equations in cylindrical coordinate system consists of equations for the conservation of time – averaged mass, momentum, and energy along with an equation of state. The use of either a differential or control volume representation for the governing equations is determined by whether a finite-difference or finite-volume discretization is being used for the numerical solution.

The primary variables of the governing equation in two dimensions are density, two components of velocity, total energy, pressure, total enthalpy, six components of the turbulent Reynolds stress tensor, and the two component of turbulent heat – flux.

3.6.1.a.Continuity Equation: -

The general continuity equation in tensor notation is expressed as:-

$$\frac{\partial \rho}{\partial t} + \frac{\partial}{\partial x_i}(\rho u_i) = S_m \qquad (3.1)$$

The equation 3.1 is valid for both incompressible as well as compressible flow. If the flow is steady and the density of the fluid remains constant , then the continuity equation reduces to

$$\frac{\partial}{\partial x_i}(u_i) = S_m \qquad (3.2)$$

Where, ρ is the density of the fluid, $\frac{\partial}{\partial xi}$ is the divergent operator, u_i is the velocity vector of the fluid and S_m is the source term.

3.6.1.b. Momentum equation: - The conservation of momentum in an inertial reference frame in Cartesian coordinate system is expressed as:-

$$\frac{\partial}{\partial t}(\rho u_i) + \frac{\partial}{\partial x_j}(\rho u_i u_j) = -\frac{\partial p}{\partial x_j} + \frac{\partial \tau_{ij}}{\partial x_j} + \rho g_i + F_i \qquad (3.3)$$

Where p is the static pressure, ρg_i is the gravitational body force, F_i is the external body force and τ_{ij} is the stress tensor (which is expressed as below).

$$\tau_{ij} = \left[\mu \left(\frac{\partial u_i}{\partial x_j} + \frac{\partial u_j}{\partial x_i} \right) \right] - \frac{2}{3} \mu \frac{\partial u_i}{\partial x_j} \delta_{ij} \qquad (3.4)$$

Where μ is the molecular viscosity and the second term on the right hand side is the effect of volume dilation and δ_{ij} is the Kronecker's delta.

The value of δ_{ij} = 0 if, $i \neq j$

= 1 if, i=j.

3.6.1.c. Energy equation: - The conservation of energy equation is expressed as:-

$$\frac{\partial}{\partial t}(\rho E) + \frac{\partial}{\partial x_i}(u_i(\rho E + p)) = \frac{\partial}{\partial x_i}\left(k_{eff} \frac{\partial T}{\partial x_i} - \sum_{j'} h_{j'} j_{j'} + u_j (\tau_{ij})_{eff} \right) + S_h \qquad (3.5)$$

Where k_{eff} is the effective conductivity ($k+k_t$, where k_t is the turbulent thermal conductivity) and $j_{j'}$ is the diffusion flux of species j'. The first three terms on the right hand side of energy equation represent energy transfer due to conduction, species diffusion and viscous dissipation respectively. S_h source term if any includes heat of chemical reaction.

The energy term 'E' is further expanded as

$$E = h - \frac{p}{\rho} + \frac{u_i^2}{2} \qquad (3.6)$$

Where sensible enthalpy 'h' is defined as

For ideal gases

$$h = \sum_{j'} m_{j'} h_{j'} \tag{3.7}$$

And for incompressible flows

$$h = \sum_{j'} m_{j'} h_{j'} + \frac{p}{\rho} \tag{3.8}$$

$m_{j'}$ is the mass fraction of species j' and enthalpy $h_{j'}$ is expressed as

$$h_{j'} = \int_{T_{ref}}^{T} c_{p,j'} dT \tag{3.9}$$

In addition to the above three basic equations of flow, some other equations are also solved depending on the nature of flow phenomenon involved in the problem. For example, if swirling flow takes place in the flow domain, then axial and radial momentum conservation equations are to be solved, where the swirl velocity is included in the equation. Similarly, viscous heating (dissipation) is important for compressible flows, PDF model in energy equation for combustion process, energy source term for chemical reactions, Boussinesq model for natural convection etc. The numerical solution of the three basic equations of fluid flow gives a close approximation to the flow problem for a steady and laminar flow. Most of the flow occurring in nature and engineering applications is turbulent. So treatment for turbulence is required to have better solution to the problem.

3.6.2 Discretization of the Governing Equations: -

The governing equations may be discretized into either a finite-difference, or finite-volume method. Fluent^{TM} uses finite volume method because of its suitability to fluid flow. Finite-difference method approximates the derivatives in the differential form of the governing equations by difference expressions formulated at discrete points in space. Because the finite difference method relies on the construction of differences between adjacent points, it requires the use of a structured computational grid. This ensures that mass, momentum and energy are conserved in the discretized formulation. Because the finite-volume method utilizes a control volume concept, arbitrary computational shape and size may be accommodated.

Finite volume schemes are gaining widespread usage today for turbomachinery CFD applications, replacing the previously dominant finite-difference discretization, because of their improved ability to conserve mass, momentum and energy, relative to the finite difference methods. The flexibility afforded by the use of arbitrary computational grids is also a distinct advantage for this method.

3.6.2.a.Numerical Solution Techniques: - The subject of numerical solution technique is too extensive to be covered in this chapter. Only a cursory discussion of methods appropriate to the solution of the time-dependent RANS equations is given.

FLUENT 6.0.1 allows to chose either of two numerical methods: *Segregated solver, or Coupled solver.*

The two numerical methods employ a similar discretization process (finite-volume), but the approach used to linearize and solve the discretized equations is different.

(i) Using *Segregated solver* approach, the governing equations are solved sequentially (i.e., segregated from one another). Because the governing equations are non-linear (and coupled), several iterations of the solution loop must be performed before a converged solution is obtained.

(ii) The *coupled solver* solves the governing equations of continuity, momentum, and energy simultaneously (i.e., coupled together). Because the governing equations are non-linear (and coupled), several iterations of the solution loop must be performed before a converged solution is obtained.

The manner in which the governing equations are linearized may take an ``implicit" or ``explicit" form with respect to the dependent variable (or set of variables) of interest. By implicit or explicit we mean the following: -

(a) Implicit: - For a given variable, the unknown value in each cell is computed using a relation that includes both existing and unknown values from neighboring cells. Therefore each unknown will appear in more than one equation in the system, and these equations must be solved simultaneously to give the unknown quantities.

(b) Explicit: - For a given variable, the unknown value in each cell is computed using a relation that includes only existing values. Therefore each unknown will appear in only one equation in the system and the equations for the unknown value in each cell can be solved one at a time to give the unknown quantities.

Both methods offer similar levels of accuracy and have been applied successfully for turbomachinery flow analysis. However, explicit methods tend to require less omputational time and are better suited for application on parallel-processor computers.

3.6.3 Turbulence Models: -

Turbulent flows are highly irregular, unsteady, chaotic and always occur at high Reynolds number. Turbulence is rotational and three dimensional and it is characterized by high level of fluctuating vorticity. Turbulent flows are characterized by fluctuating velocity fields. These fluctuations mix transported quantities such as momentum, energy and species concentration and cause the transported quantities to fluctuate. The instabilities are related to the interaction of viscous terms and non linear inertia terms in the equations of motion. This interaction is very complex: the mathematics of non linear partial differential equation has not been developed to a point where general solutions can be given. The fluctuation of the transported quantities are of small scale and high frequency, they are too computationally expensive to simulate directly in practical engineering calculations. So the instantaneous governing equations are time averaged, ensemble-averaged, or otherwise manipulated to remove the small scales, which give a modified set of equations which are less expensive to solve numerically. But the modified equations contain additional unknown variables for which turbulence models are required to determine these unknown quantities in terms of known quantities.

The most common used approach to address the turbulence effect on flow is the Reynolds-Averaged Navier-Stokes equations (RANS). They represent transport equations for the mean flow quantities only, with all the scales of the turbulence being modeled. The approach of permitting a solution for the mean flow variable greatly reduces the computational effort. A computational advantage is seen even in transient situations, since the time step will be determined by the global unsteadiness in the

mean flow rather than by the turbulence. This approach is generally adopted for engineering calculations.

In RANS approach, the solution variables in the instantaneous Navier-Stokes equations are decomposed into the mean (ensemble-averaged or time averaged) and fluctuating components. The velocity component in tensor notation (3d) is expressed as

$$u_i = \overline{u_i} + u_i' \tag{3.10}$$

Where $\overline{u_i}$ and u'_i are the mean and instantaneous velocity components

Similarly for scalar quantities:

$$\phi = \overline{\phi} + \phi' \tag{3.11}$$

Where ϕ denotes a scalar quantity such as pressure, energy, species concentration.

Putting the values of flow variable into the instantaneous continuity and momentum equation, the simplified equations are expressed as:

$$\frac{\partial \rho}{\partial t} + \frac{\partial}{\partial x_i}(\rho u_i) = 0 \tag{3.12}$$

$$\rho \frac{Du_i}{Dt} = -\frac{\partial p}{\partial x_i} + \frac{\partial}{\partial x_j}\left[\mu\left(\frac{\partial u_i}{\partial x_j} + \frac{\partial u_j}{\partial x_i} - \frac{2}{3}\delta_{ij}\frac{\partial u_l}{\partial x_l}\right)\right] + \frac{\partial}{\partial x_j}\left(-\rho\overline{u_i' u_j'}\right) \tag{3.13}$$

The above continuity and momentum equations have the same general form as the instantaneous Navier-Stokes equations. Additional terms now appear that represent the effects of turbulence, is called Reynolds stresses, $\rho\,\overline{u'_i\, u'_j}$ and must be modeled in order to close the modified momentum equation.

"Turbulence modeling concerns itself with the generation and testing of closure relations describing the Reynolds stresses". Since its inception the goal of turbulence

modeling has been the development of a “universal model” which can describe the Reynolds stresses of any turbulent flow without any previous experimental information. Such a model does not at yet exit and, in fact, may never exit. The few predictable flows fall into the category of equilibrium flows, which in turn may be defined as flows in which the production and dissipation of turbulence energy, shear stresses etc. are in balance. Examples of such flows are boundary layers on mild curvature at subsonic speed, shock-free supersonic flows, far wakes and mixing layers well downstream of their initiation.

The complete discussion of the mathematics of turbulence modeling is out of the scope of this study. So different types of turbulence model available in Fluent 6.0.1 and used in this simulation has been discussed. Fluent 6.0.1 provides the following choices of turbulence models: -

(i) Spalart - Allmaras model (One equation)

(ii) κ–ϵ models (Two equations)

(a) Standard κ–ϵ model

(b) Renormalization-group (RNG) κ–ϵ model

(c) Realizable κ–ϵ model

(iii) κ-ω models (Two equation)

(a) Standard κ-ω model

(b) Shear-stress transport (SST) κ-ω model

(iv) v^2 - f model

(v) Reynolds stress model (RSM) (seven equations)

(vi) Large eddy simulation (LES) model

It is an unfortunate fact that no single turbulence model is universally accepted as being superior for all classes of problems. The choice of turbulence model depends on considerations such as the physics encompassed in the flow, the established practice for a specific class of problem, the level of accuracy required, the available computational resources, and the amount of time available for the simulation. In the present study RNG κ–ϵ and κ-ω SST (shear stress Transport) turbulence models were chosen because of their better capability to predict wall-bounded flows like turbine flow. RNG κ–ϵ model was selected because it is most popular in the current CFD simulation scenario while κ-ω SST was chosen to see if there is any variation in the results predicted by the RNG κ–ϵ. Eventually no significant change was found in the predictions made by the two models. Finally it was decided to do the simulation with RNG κ–ϵ turbulence model.

RNG *κ–ϵ* turbulence model: -

The standard *κ*–ϵ turbulence model is a Reynolds-averaged Navier-Stokes (RANS) model with two transport equations—one for the turbulent kinetic energy (*k*) and one for the eddy viscosity (ϵ*)* which are used to approximate the turbulent viscosity (μ_t)

The RNG *k*- ϵ model involves renormalization group theory and adds a term to the eddy viscosity transport equation, which makes the model better for high strain flows than the standard *k*- ϵ model. One major drawback of the RNG *k*- ϵ model in wall-bounded flows, such as film cooling, is the assumption of isotropic turbulence. The existence of the wall introduces anisotropy in the normal fluctuations, the presence of which are not

accounted for in the wall functions used to approximate the behavior in the boundary layer in the *k*- ϵ turbulence models. Wall functions lose their reliability in three-dimensions or separated flow regimes, such as sometimes seen in film cooling

The RNG κ– ϵ turbulence model is derived from the instantaneous Navier-Stokes equations, using a mathematical technique called ``renormalization group'' (RNG) methods. The analytical derivation results in a model with constants different from those in the standard κ–ϵ model, and additional terms and functions in the transport equations for κ and ϵ.

Transport Equations for the RNG κ– ϵ Model: -

The RNG based κ– ϵ model has a similar form to the standard based κ– ϵ model:

$$\frac{\partial}{\partial t}(\rho k) + \frac{\partial}{\partial x_i}(\rho k u_i) = \frac{\partial}{\partial x_j}\left(\alpha_k \mu_{\text{eff}} \frac{\partial k}{\partial x_j}\right) + G_k + G_b - \rho\epsilon - Y_M + S_k \qquad 3.14$$

$$\frac{\partial}{\partial t}(\rho\epsilon) + \frac{\partial}{\partial x_i}(\rho\epsilon u_i) = \frac{\partial}{\partial x_j}\left(\alpha_\epsilon \mu_{\text{eff}} \frac{\partial \epsilon}{\partial x_j}\right) + C_{1\epsilon}\frac{\epsilon}{k}(G_k + C_{3\epsilon}G_b) - C_{2\epsilon}\rho\frac{\epsilon^2}{k} - R_\epsilon + S_\epsilon$$

…3.15.

In these equations, G_κ represents the generation of turbulence kinetic energy due to the mean velocity gradients. G_b is the generation of turbulence kinetic energy due to buoyancy. *Ym* represents the contribution of the fluctuating dilatation in compressible turbulence to the overall dissipation rate. The quantities α_κ and α_ϵ are the inverse effective Prandtl numbers for κ and ϵ, respectively. S_κ *and* S_ϵ are user-defined source term.

3.7 Figures: -

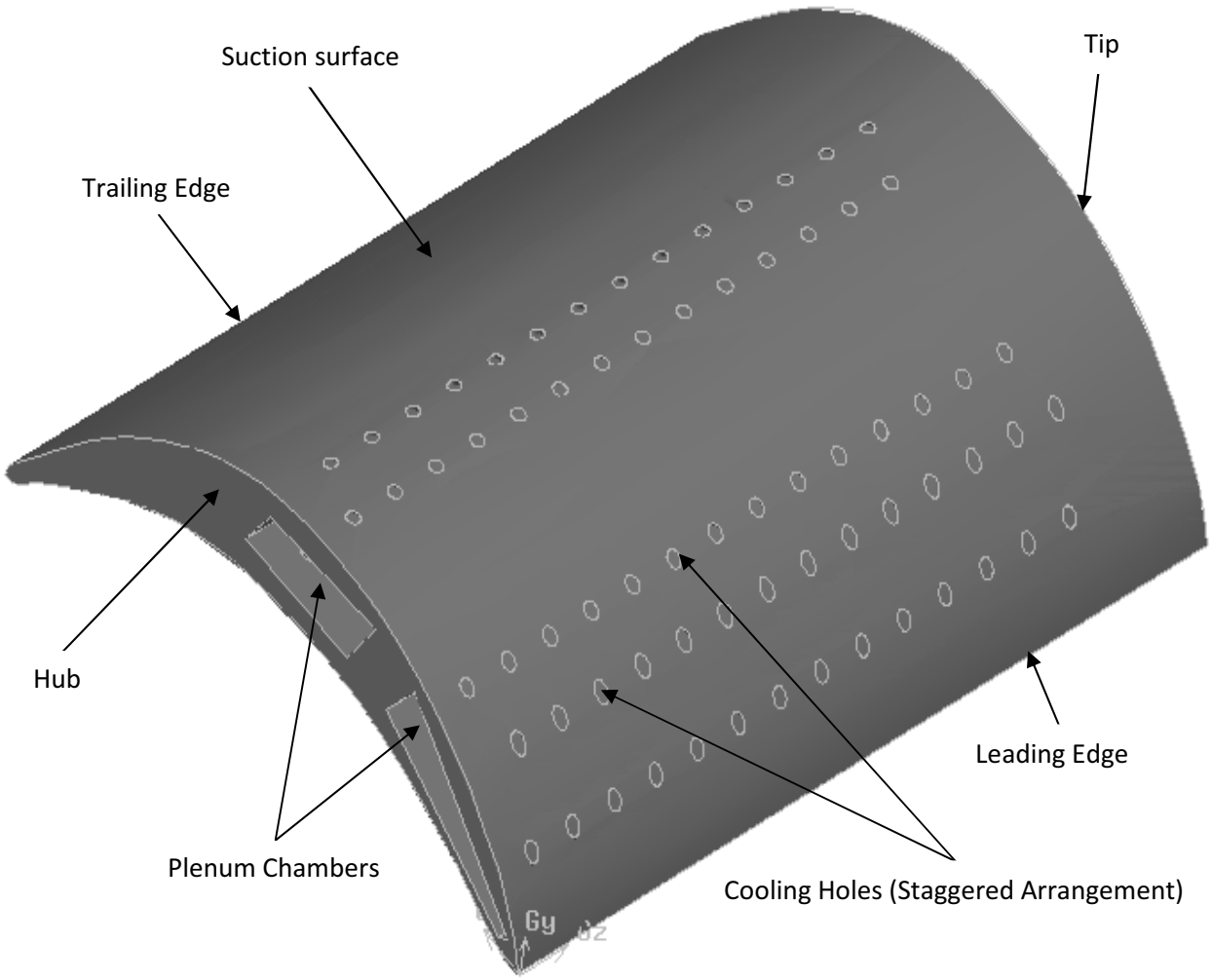

Fig. 3.1: 3-D Cascade showing plenum chambers and film cooling holes on the suction side (solid model).

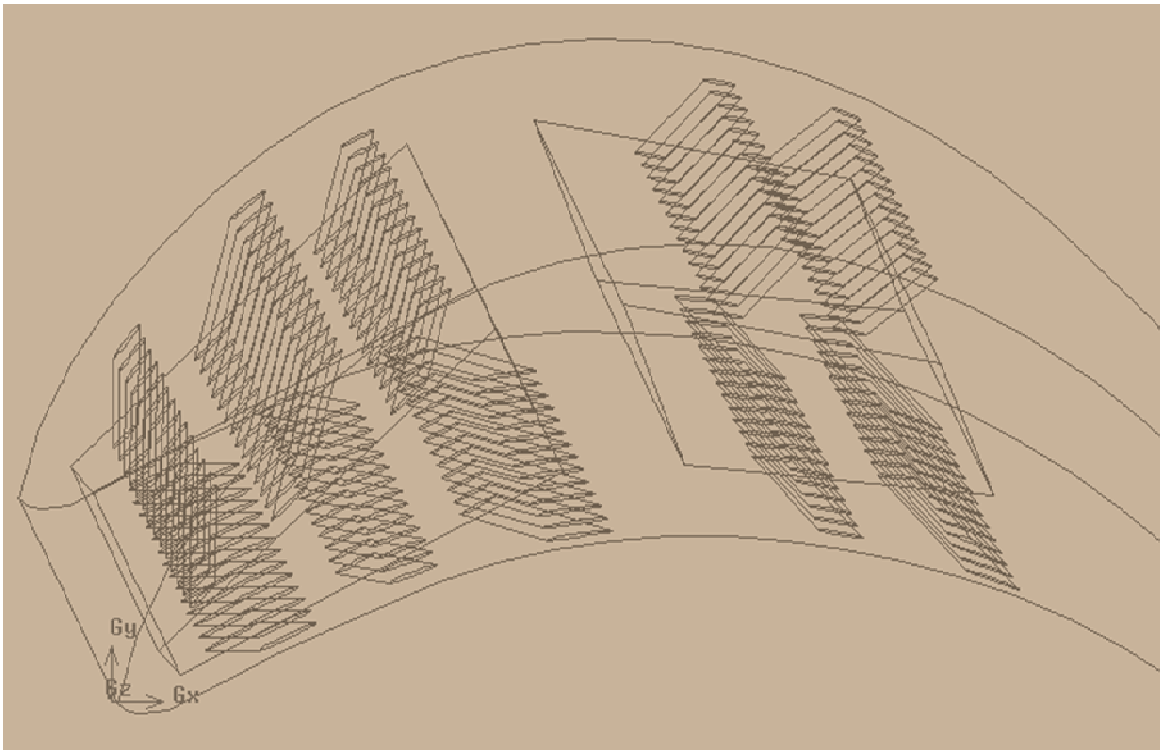

Fig. 3.2: Wireframe model (pressure side).

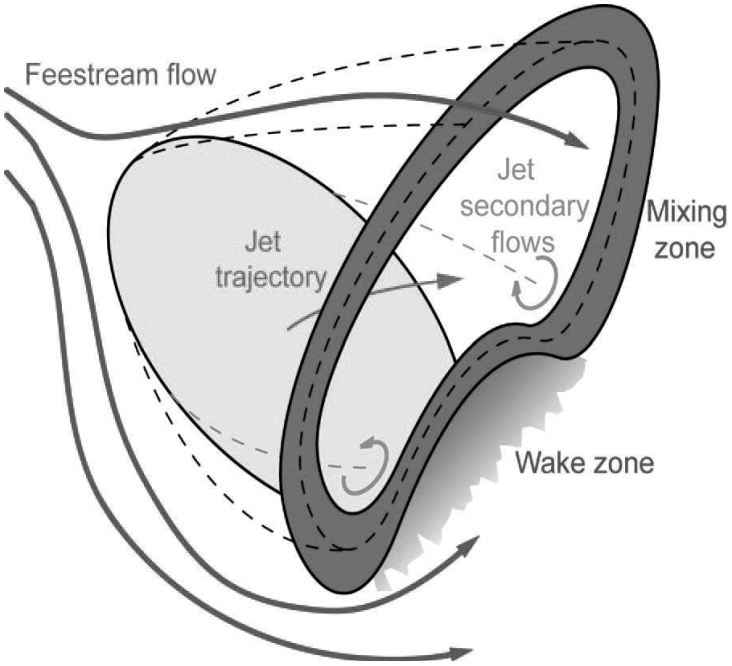

Fig. 3.3: Sketch of the near hole region [4].

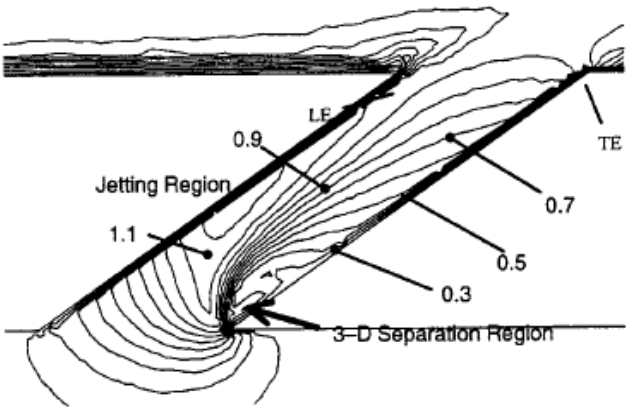

Fig. 3.4: Velocity magnitude showing jetting and separation region [12]

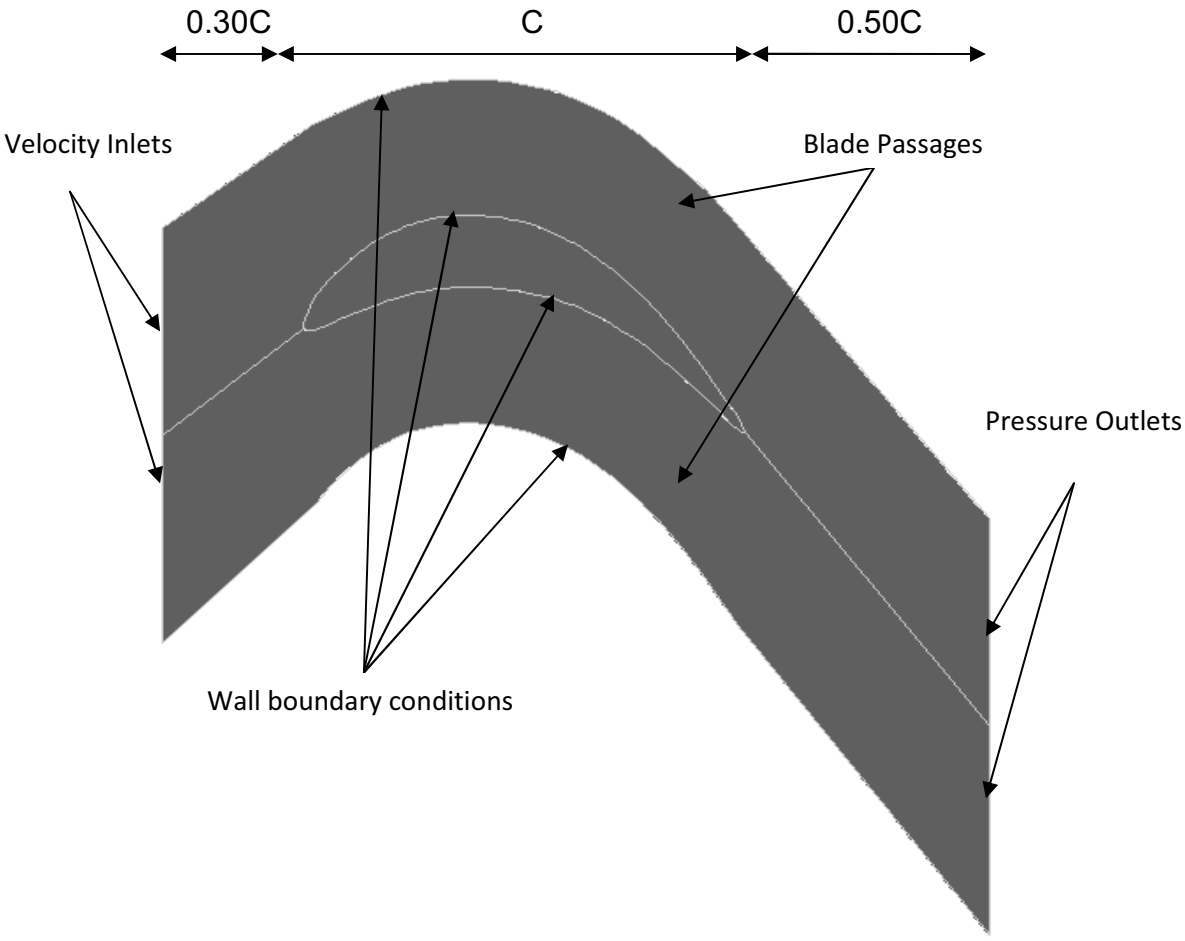

Fig. 3.5: 2-D view of the CFD domain (uncooled blade)

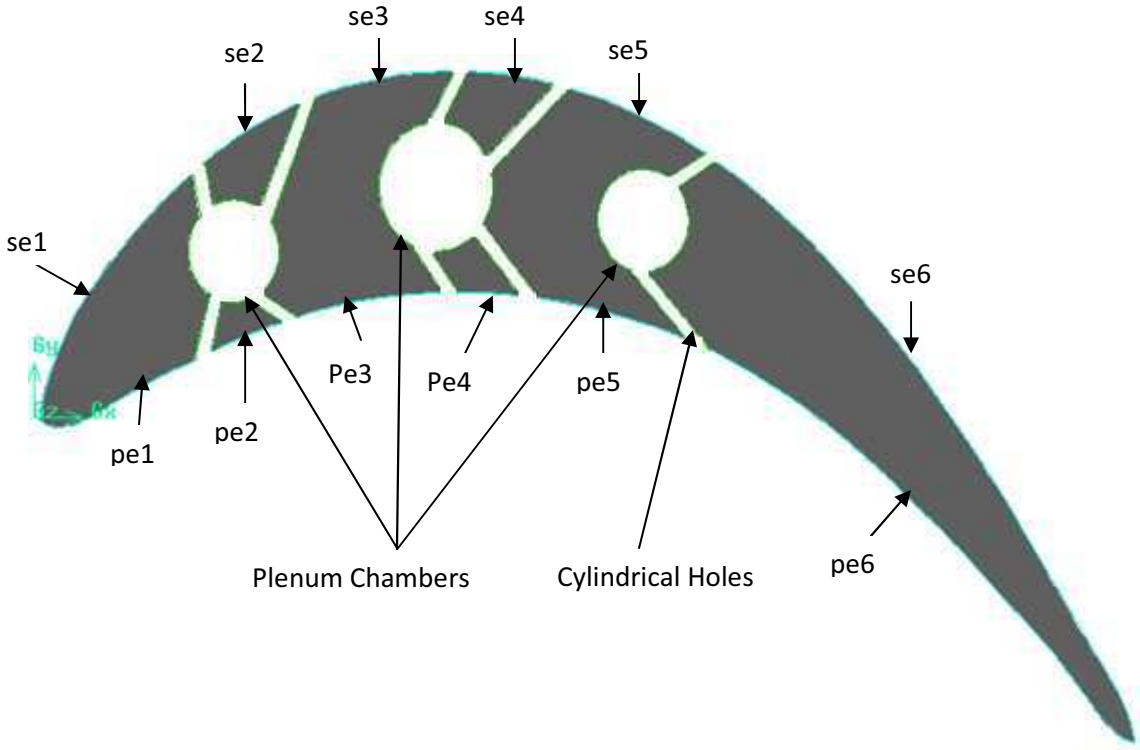

Fig 3.6: Vane with cylindrical film-cooling holes and plenum chambers.

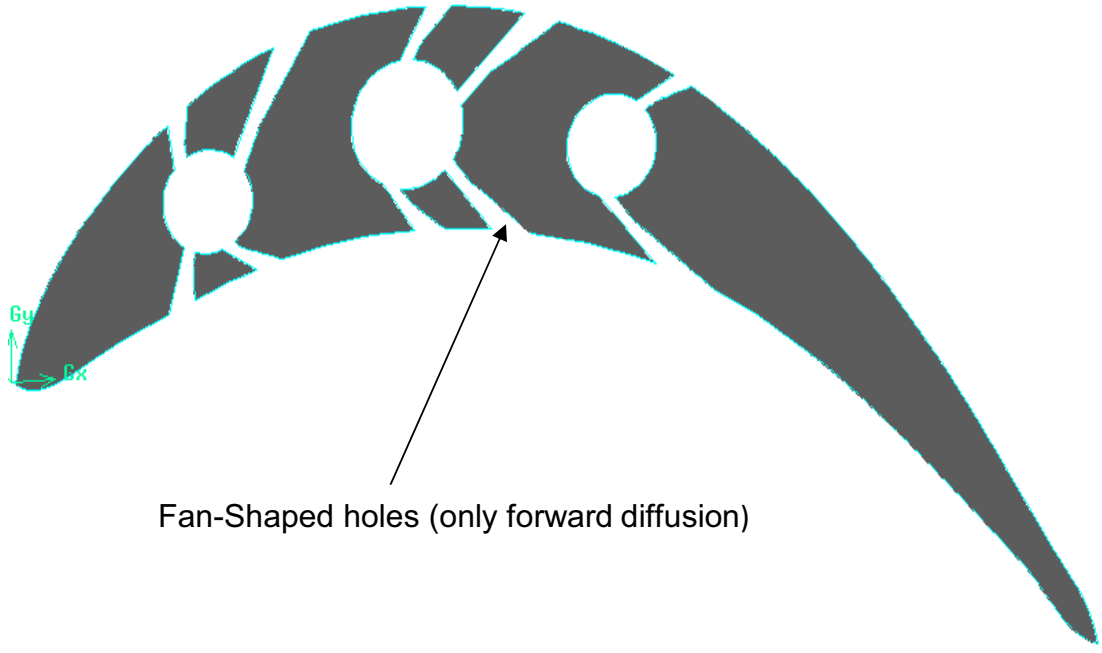

Fig. 3.7: Vane showing fan shaped holes

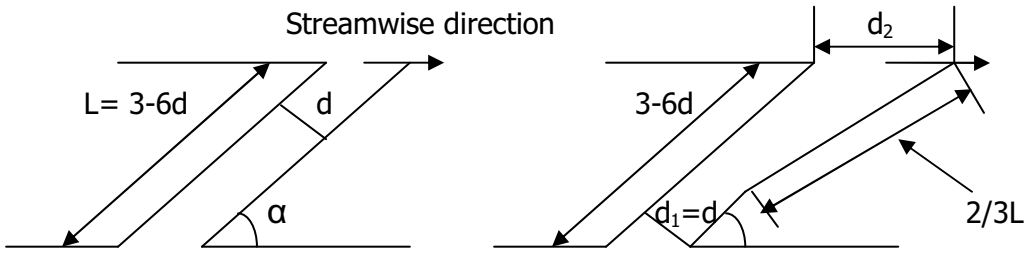

(a) Round Hole (b) Shaped Hole

Fig. 3.8: Main geometrical parameters of the cooling hole.

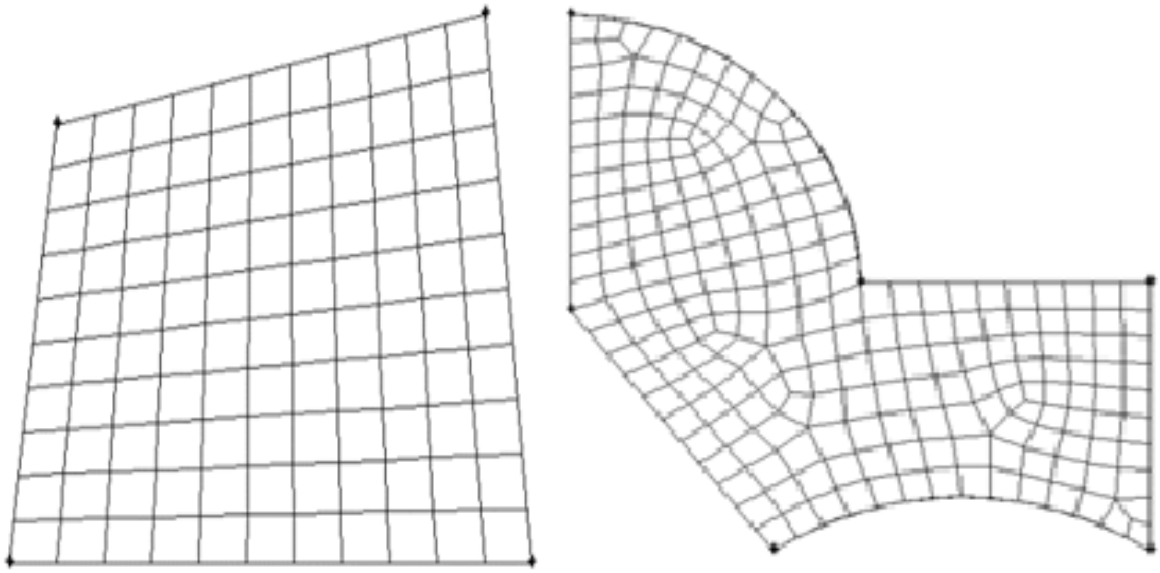

(a) Structured Grid (b) Unstructured Grid

Fig. 3.9: Illustration of structure and unstructured grids.

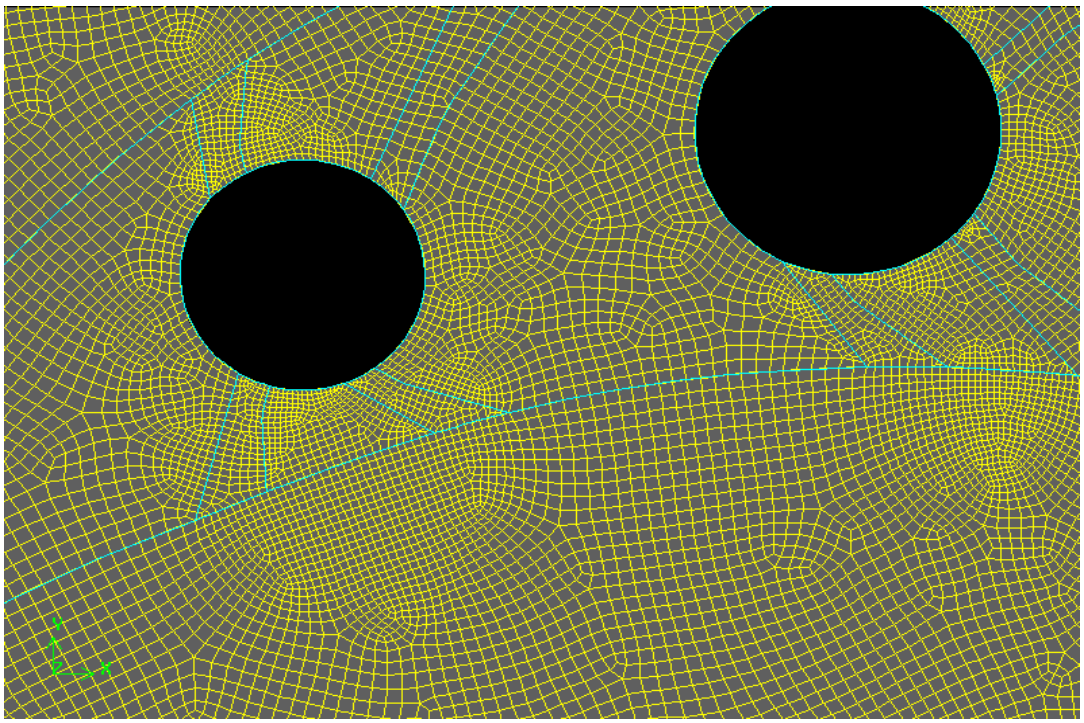

Fig. 3.10: Unstructured grid of the vane showing high grid density at the near hole region and comparatively lower density grid away from the hole region.

4.1 Uncooled Blade Predictions: -

Initially simulation was done for uncooled condition in order to give an overview of the flow and temperature distribution around the blade. Fig. 4.1 shows contours of the static pressure distribution over the entire computational domain.

In the upstream region, higher pressure is depicted by the yellow colour contours. Stagnation point has been shown indicating the maximum pressure region which is in consistent with the reality. As the flow proceeds, it accelerates in the converging portion of the cascade and the pressure increases in the mid region of the flow path as shown by the green colour contours. On the suction and pressure sides, negative and positive pressure regions respectively are shown by the blue colour contours. In the downstream side of the trailing edge the intermixing of the core flow and the wake takes place and the total pressure drops.

The velocity vectors are shown in fig. 4.2. The fluid moves with constant velocity up to the inlet section of the cascade. The velocity reaches its highest value when the fluid passes through the throat section of the cascade. The velocity reduces afterwards when the core flow and the flow in the wake region mix. The flow further reduces in the diverging portion of the model before finally leaving the domain.

Cooled Blade Predictions: -

The predictions of the temperature distribution and flow structures of the simple cylindrical hole and fan-shaped holes for low, moderate and high blowing ratio have

been presented and discussed. Besides, the effect of free-stream turbulence for moderate and high blowing ratio has been studied.

4.2. Investigations of Simple Cylindrical Holes: -

4.2.1 Low Blowing Ratio, M=0.18: -

Fig. 4.3 shows the temperature contours for low value of blowing ratio (M=0.18). Since there is no cooling in the leading edge and trailing edge of the blade, temperature in this region is relatively higher. The temperature of the portion of the blade containing the film cooling holes is comparatively lower. The heat transfer from the mainstream gas to the blade is prevented by the coolant jet ejecting from the cooling hole and forming a thin film on the surface. At any section of the blade in the y-direction, the temperature is constant throughout the blade thickness which is not true in practice. It should also be noted that film cooling downstream of the every holes is strongly influenced by the proximity of the previous hole.

(a) *Suction side cooling: -*

The static temperature variation of the suction side of the vane is shown in fig. 4.4. As shown, static temperature is varying from a maximum of 450 K on the leading edge (se1) to a minimum of 320 K on the edge se4. The temperature of the edge se3 is little lower than the edge se2 which is attributed to increase in the streamwise pitch distance (from 6 to 7 hole diameters) between the holes. Edge se4 has the lowest pitch distance (5d) and arguably showing the minimum temperature ~320 K. In the downstream side, the trailing edge se5 is showing a relatively steep increase in temperature (~420 K). This is because of the combined effect of the higher pitch distance, low length-to-diameter ratio, higher injection angle (higher injection angle

leads to detachment of the coolant from the surface and greater mixing with the freestream gas and hence more heat transfer), and absence of cooling hole. Also, all holes exhibited a relatively flat temperature profile in the streamwise direction.

(b) *Pressure side cooling:* -

Fig 4.5 shows the temperature variation of the pressure side edges designated as pe1 to pe6 from the leading edge. Pressure side cooling exhibited a trend little different than the suction side. Temperature are bit lower (10-50 K), as the velocity of the gas is lower than the suction side and so mixing will be less. Edge pe4 is showing a minimum temperature ~315 K owing to the extremely close hole spacing (4d). Trailing edge temperatures are same as that of se6.

(c) Streamlines inside the Hole and at the Downstream of the Ejection Location: - Fig. 4.6 shows the vectors of velocity in the near hole region which is the main area of interest because of its substantial influence on the film cooling performance.

For blowing ratio is low (M = 0.18), the width of jet contour on the ejection site is very thin because of lesser mass flux coming out from the hole. Because of the low momentum flux the coolant jet is not able to penetrate into the mainstream hot gas. At the outside of the hole, there is a deflection of the mainstream flow towards the gas path side and coolant flow towards the wall side because of interaction of the momentum of the coolant jet with that of the hot gas. However, the interaction is not so severe because of the lesser mass flux. One advantage of the low blowing ratio is that the streamlines remained attached to the edge because of the lower normal momentum which reduced the heat transfer to the vane.

4.2.2 Moderate Blowing Ratio, M = 0.5: -

(a) *Fig. 4.7 shows the temperature contours of the complete domain for moderate value of blowing ratio of M = 0.5*: -

With the increase in blowing ratio the width of the coolant boundary layer around the vane has increased as depicted in the fig. 4.7. This is because of the higher momentum and mass flux of the coolant coming out of the holes. This directly insulates the vane from the heat of the mainstream gas resulting into better cooling and hence better protection of the vane.

(b) *Temperature distribution of the inside of the vane surface at four different positions for low and moderate blowing ratio has been shown in fig. 4.8: -*

It can easily be inferred from the graphs that with the increase of blowing ratio from 0.18 to 0.5, the temperature of the vane surface comes down considerably. Even at the leading edge where there is no coolant flow, the temperature is lower than that for the low blowing ratio. At a distance of around 20 mm from the leading edge, temperature has come down to around 305 K. This finding is supported by the belief that the upstream coolant caused increased turbulent mixing in the downstream jet. This enhanced mixing caused better film-cooling jet diffusion and consequently more effective cooling. Besides, the temperature of the trailing edge has also been lowered by about 50 degree.

(c) *Temperature variation of the suction and pressure sides is shown in fig. 4.9 and 4.10 respectively: -*

It is evident from all the graphs that there is a very little or no variation of temperature in the downstream side of the holes on the pressure and suction sides.

When compared with the data in the open literature for 3D, this is over predicted; as significant variation in temperature occurs because of the mixing of the coolant with the hot gas in the downstream side of the hole.

(d) *The streamlines on the leading region of the vane is shown in fig. 4.11: -*

As shown in the fig. 4.11, significant jet lift-off has occurred at the leading edge causing poor cooling in leading edge region. Lift-off occurred because of the high surface angle of the hole which increases the normal momentum of the jet, thereby travelling more towards the mainstream side rather than remaining attached to the boundary. This has increased the temperature of the edge pe2 by about 30 K. Besides, at the near hole region flow reversal is taking place because the coolant is not able to take a sharp turn, which is around 120^{o} at the ejection location. Fig. 4.12 shows the velocity vectors at the trailing edge. As compared to the leading edge, the jet at the trailing edge shows no lift-off which is attributed to a very low injection angle of 25^{o}. As a consequence the coolant jet remains attached to the edge of the vane thereby increasing the cooling effectiveness.

4.2.3 High Blowing Ratio, M = 1: -

With the further increase in blowing ratio, there is a significant increase in jet lift-off (as shown fig. 4.13) because of the high curvature and high momentum flux which adversely affects the film-cooling performance (degradation may be about 30-40%). This decrease is because of the enhanced mixing of the coolant air with the hot gas which increases the temperature of the coolant air. The coolant flow on the suction side is completely detached and could not remain close enough to the edge on the

downstream side to have an effect, thereby allowing the mainstream gas to enter the vane surface and raising its temperature.

However, in the trailing edge jet lift-off is not so pronounced, as shown in fig. 4.14, (because of less curvature). This leads to reversal in trend of film cooling performance in the trailing edge i.e. with increase in blowing ratio, cooling effectiveness increased.

4.3 Investigation of Fan-Shaped Holes: -

The temperature distributions of the suction and pressure side at different blowing ratio have been plotted in fig.4.15a. For low blowing ratio, temperatures of the suction and pressure sides are bit higher (around 20^{o}) (fig. 4.15a and fig.4.15b) as compared to simple cylindrical holes. It is because of the very low velocity (and hence low momentum) of the coolant jet at the hole exit which reduces the ability of the jet to progress towards the downstream side of the hole. Because of the diffusive nature of the shaped holes, the velocity of the jet is low at the hole outlet. The velocity vectors for low blowing ratio can be visualized from fig. 4.16. As shown, the coolant jet velocity is very low inside the hole (depicted by very small vectors). Because of very low momentum, the jet is not able to penetrate on the edge and as a consequence cooling has been adversely affected.

But as the blowing ratio is increased from 0.18 to 0.50, the performance of the shaped hole has improved which can be seen from the temperature distribution on the suction and pressure sides in fig. 4.15c and 4.15d. The graphs show a average fall in the temperature of around 30 degree. Velocity vectors at the hole exit as shown in fig.4.17. The improvement in cooling effectiveness is attributed to increase in the

momentum of the jet (because of higher mass flux) and hence better coverage of the vane surface.

With the further increase in blowing ratio from 0.5 to 1.0, the temperatures are further reduced as shown in 4.15e and 4.15f because of greater amount of coolant. But this gain is achieved at the cost of higher jet lift-off as shown in fig. 4.18.

4.4 Effect of Free Stream Turbulence: -

At the exit of a gas turbine combustor, turbulence levels can range from 7 to 20% and vary widely with combustor geometry. This has a direct bearing on the performance of the film cooling. The effect of turbulence was studied on simple cylindrical hole by varying the turbulence intensity of the free stream from 7% to 20%. Comparison of the temperature distribution of the pressure sides for three turbulence intensity has been shown in fig.19a, 4.19b &4.19c. As shown, there is not any significant variation in temperature with the increase in blowing ratio which is not well captured well because of 2D model.

4.5 Effect of Varying the Turbine Inlet Temperature (TIT): -

In the real gas turbine engines, the temperature at the entry of the turbine may vary widely due to variation in the load. To study the effect of this variation, the turbine inlet temperature was varied from 500 K to 1100 K. The temperature distribution at the suction and pressure sides has been plotted in fig. 4.20. The graph showed similar trend as of lower TIT level, but with an increase in the value of the blade temperature. The leading edge temperature increased from 460 K for TIT of 500 K to around 1010 K for TIT of 1100 K. Minimum temperature was 400 K while the temperature varied between 400 K to 500 K for all the edges except the leading edge.

4.6 Figures: -

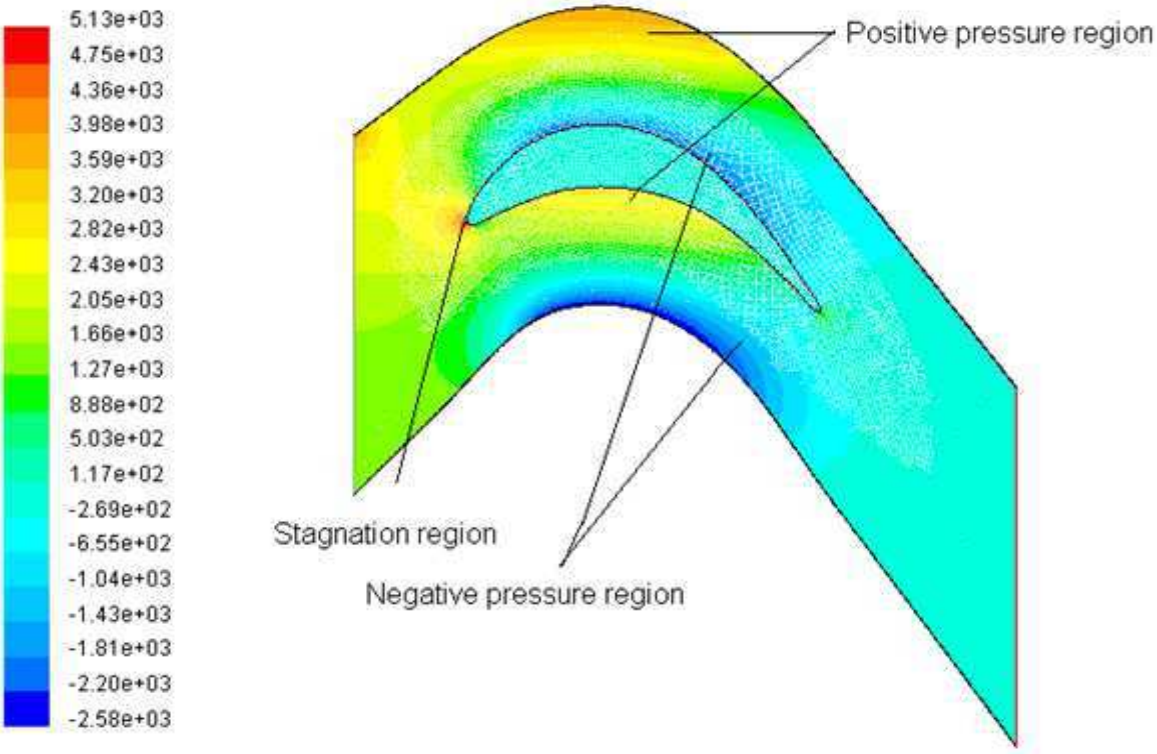

Fig. 4.1: Static pressure Contours (Pa)

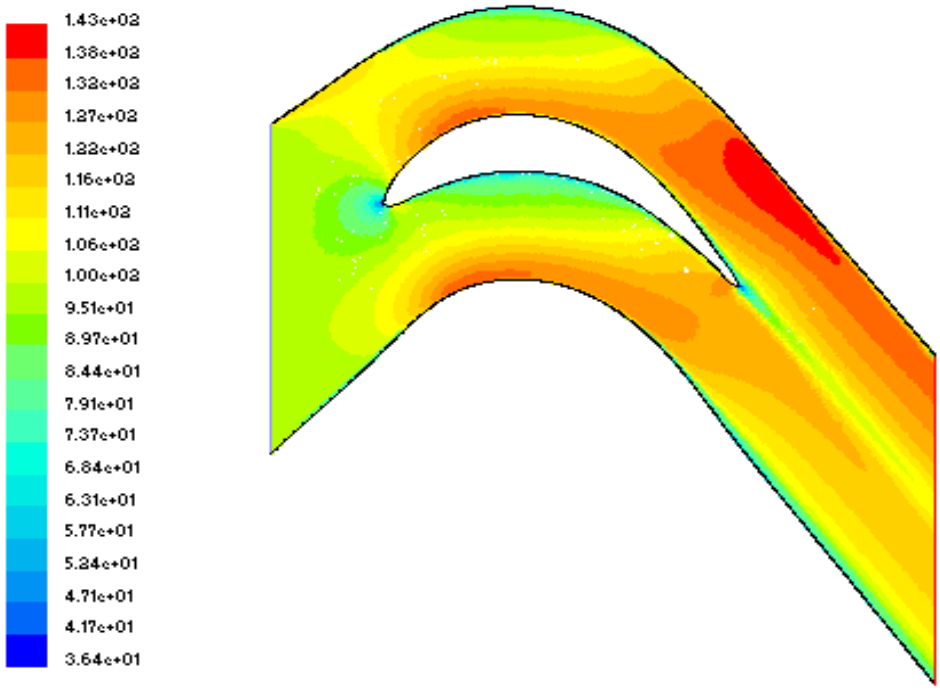

Fig. 4.2: Velocity contours (m/s)

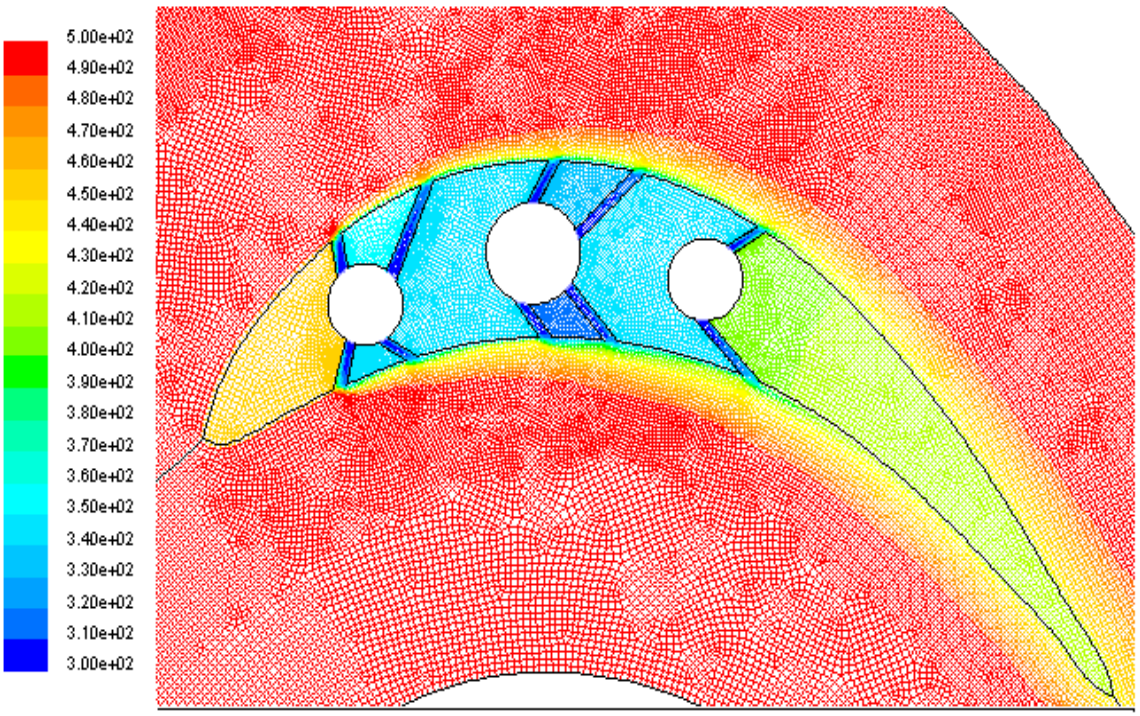

Fig. 4.3: Contours of static temperature (K)

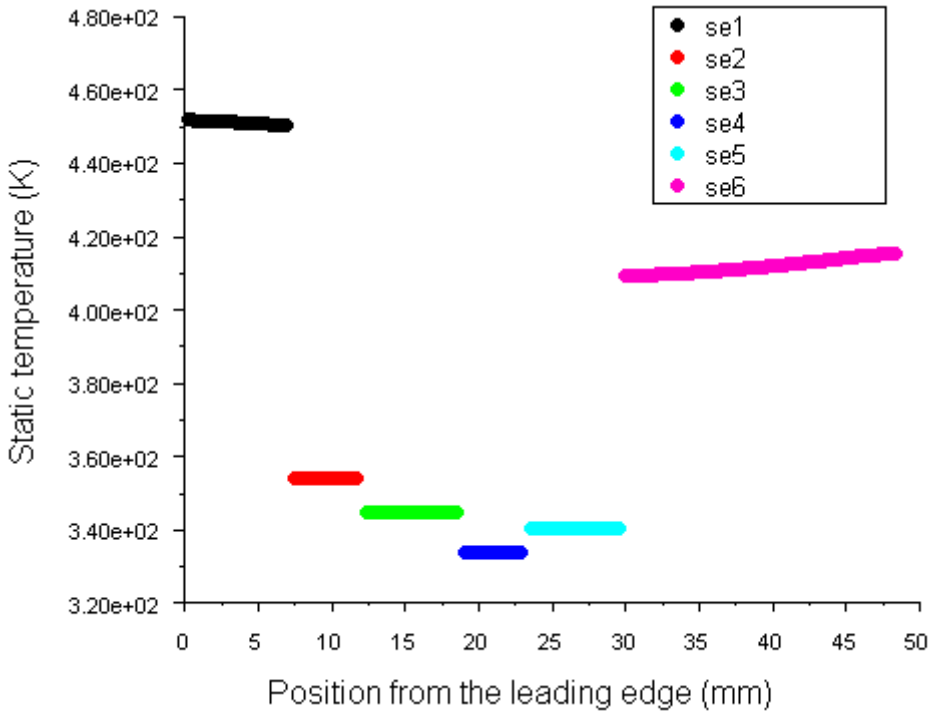

Fig 4.4: Temperature distribution of the suction side edges.

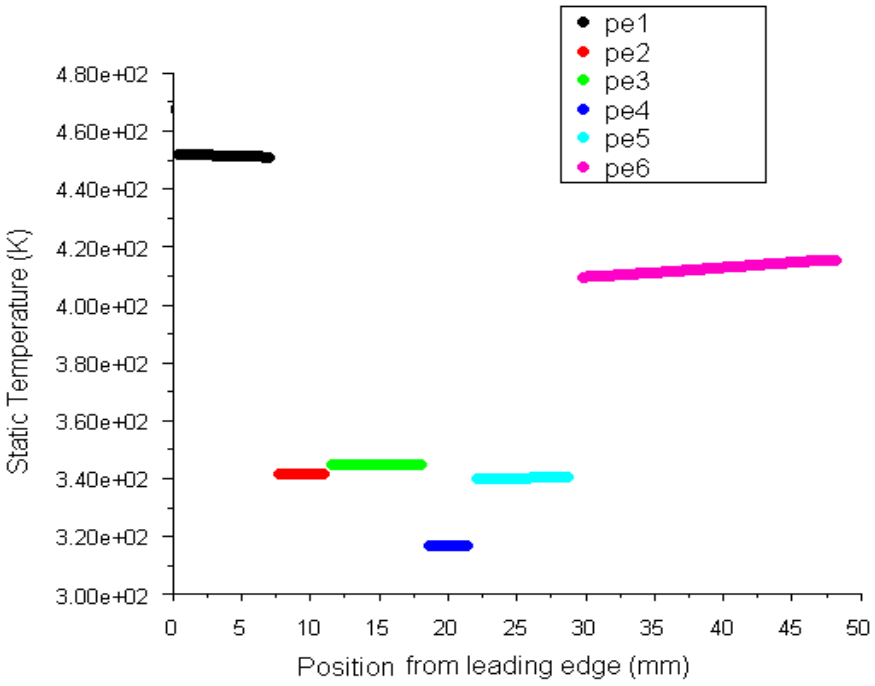

Fig. 4.5: Temperature distribution on the pressure side edges.

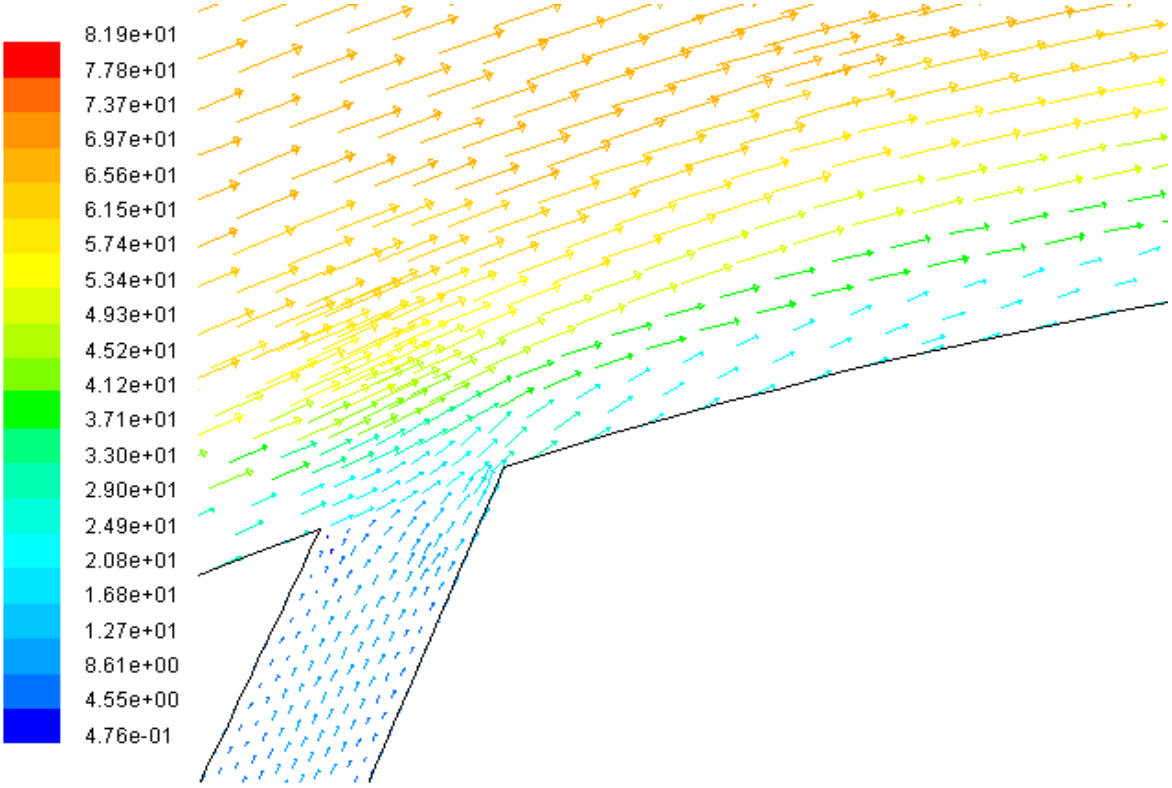

Fig. 4.6: Velocity vectors inside the hole and in the near hole region of pressure side (velocity magnitude in m/s).

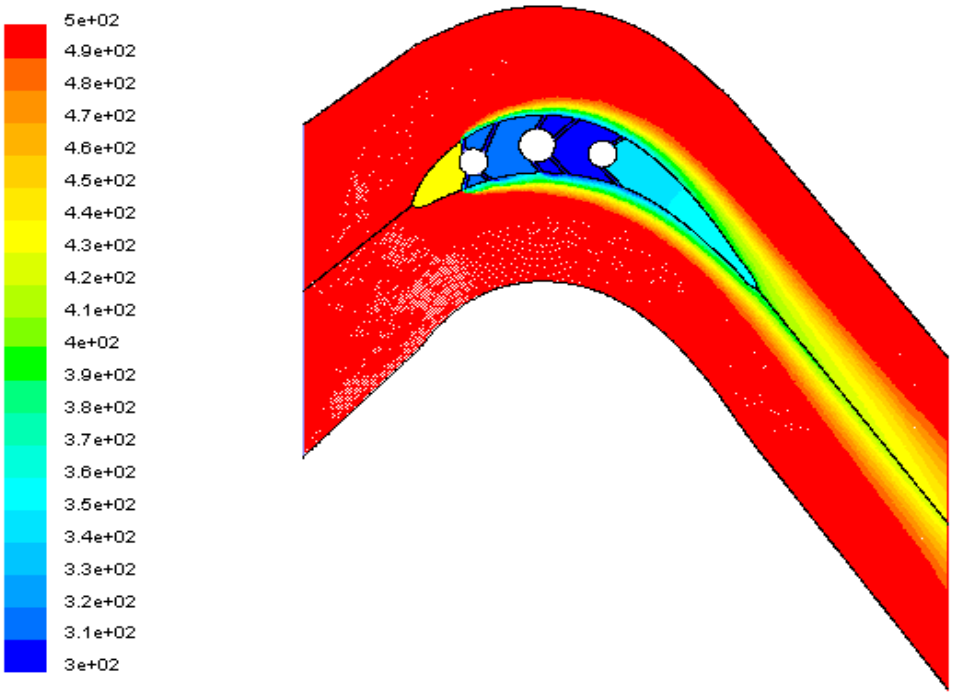

Fig. 4.7: Temperature contours for moderate blowing ratio, (M = 0.5).

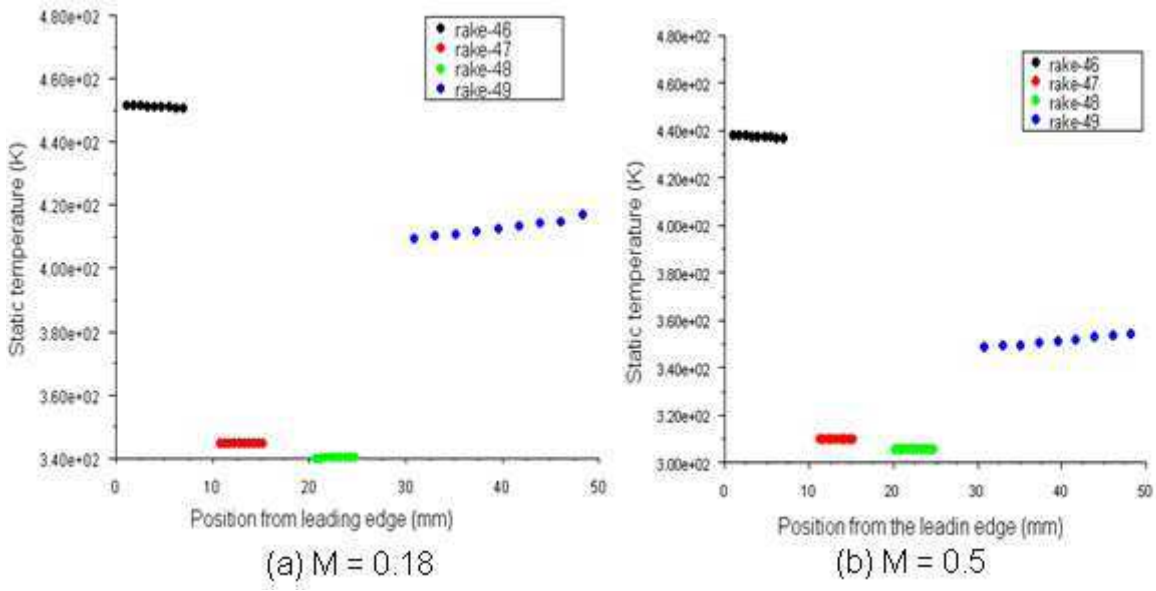

Fig. 4.8: Comparison of temperature distribution for low and moderate blowing ratios.

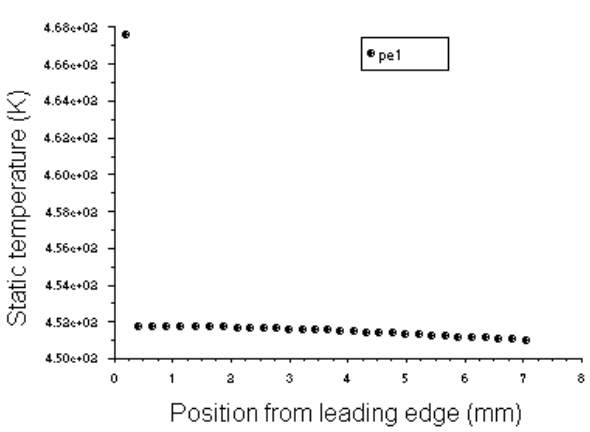

(a) Pressure edge1

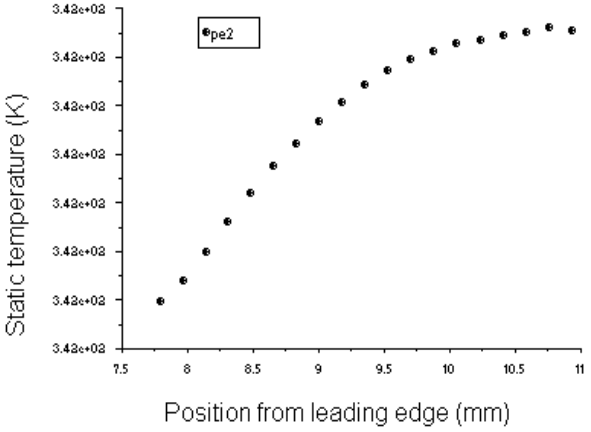

(b) pressure edge2

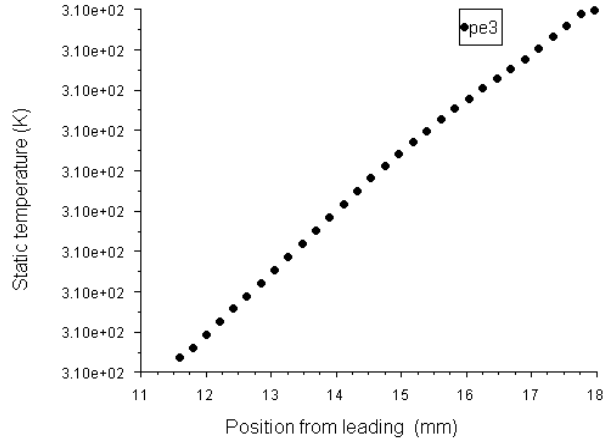

(c) pressure edge3

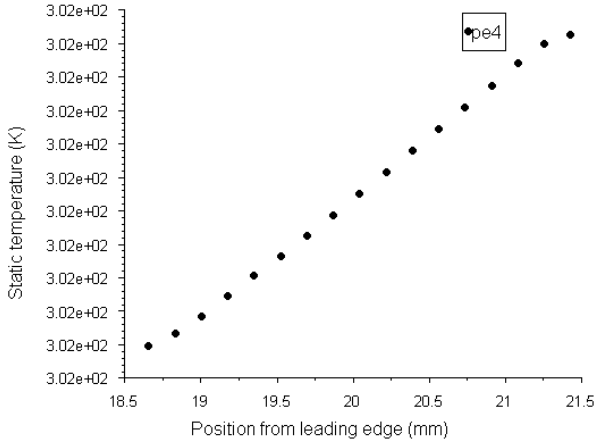

(d) pressure edge4

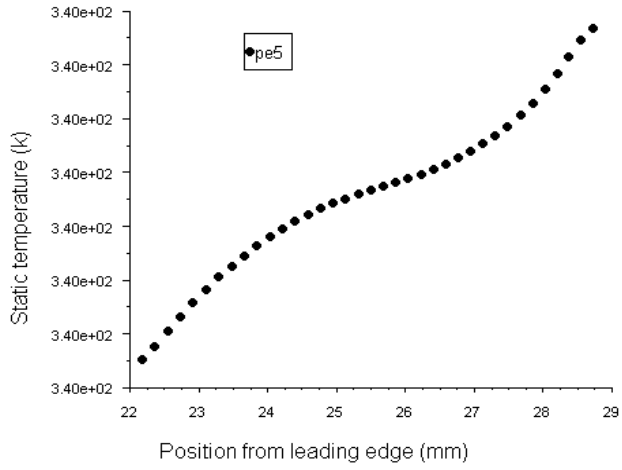

(e) pressure edge5

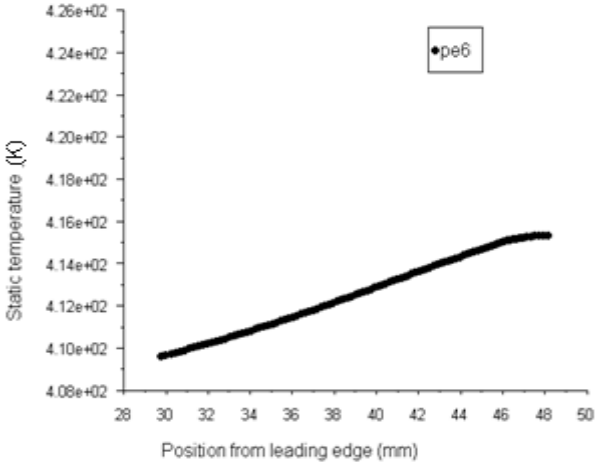

(f) pressure edge6

Fig. 4.9: Streamwise temperature variation on pressure sides; blowing ratio, M=0.5.

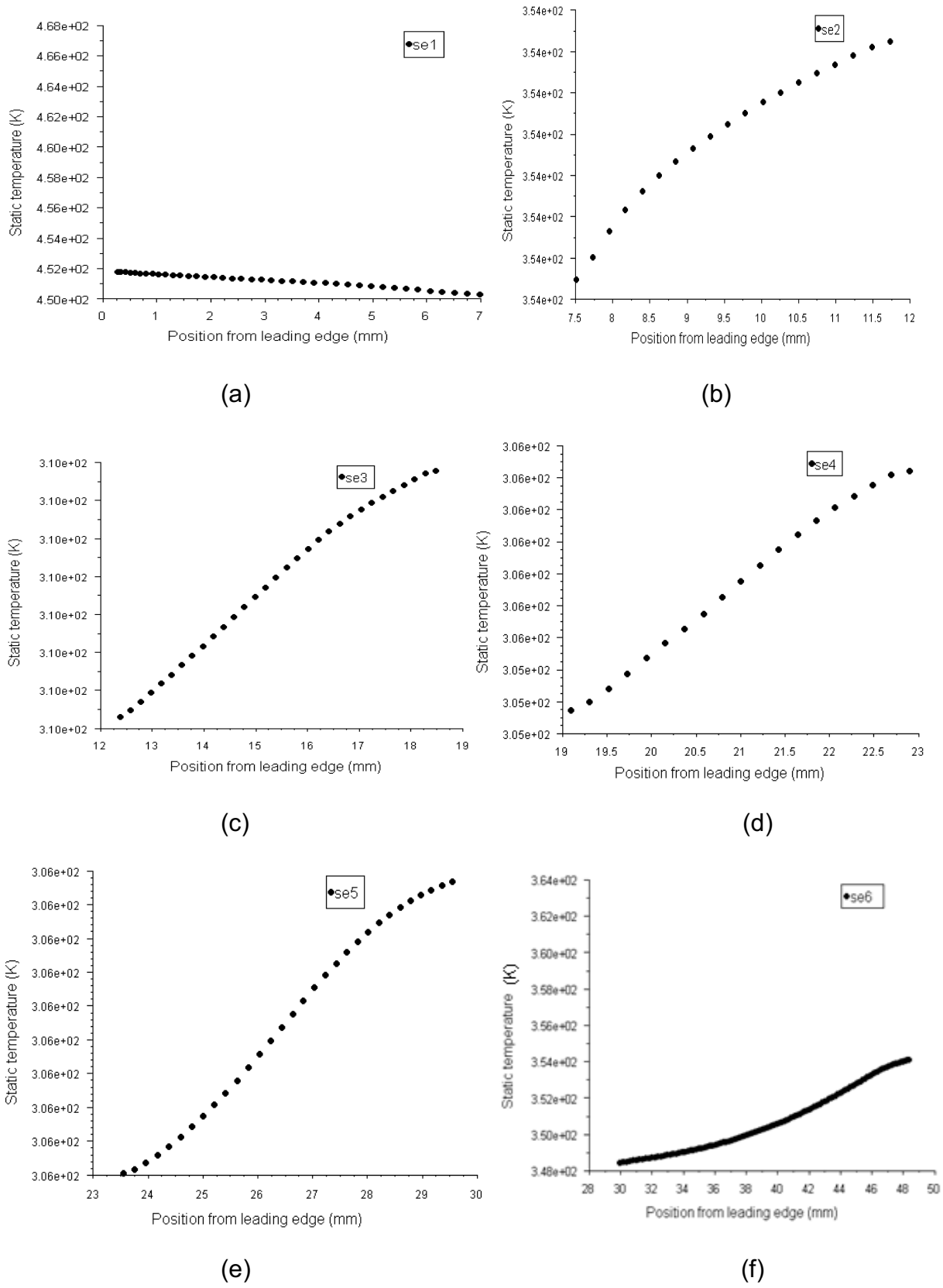

Fig. 4.10: Streamwise temperature variation on suction sides, blowing ratio, M=0.5.

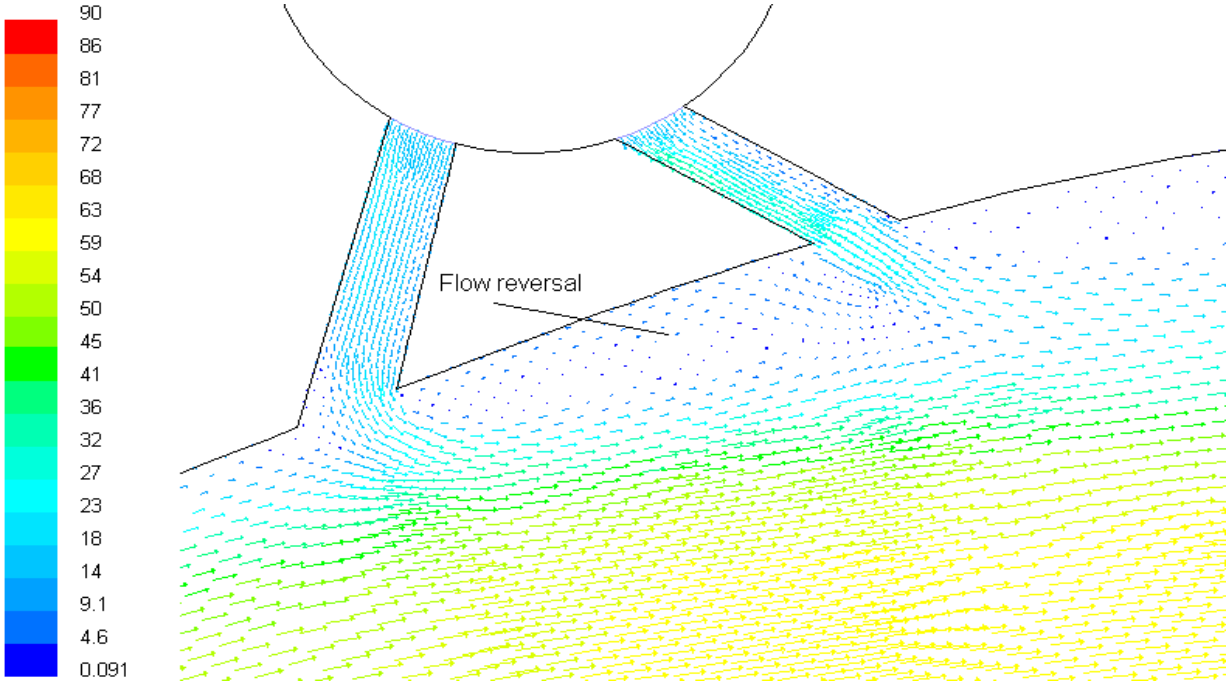

Fig. 4.11: Velocity vectors at the leading edge region of pressure side (velocity in m/s); blowing ratio, M =0.5.

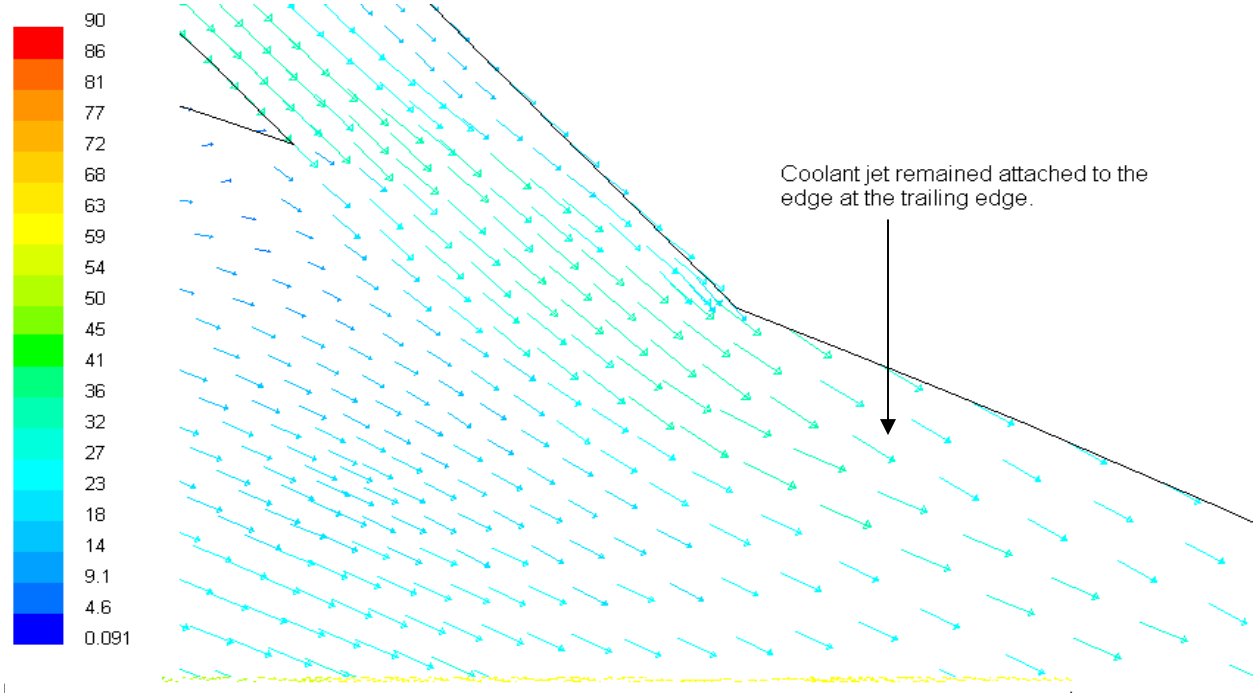

Fig. 4.12: Velocity vectors at the trailing edge region (velocity magnitudes in m/s).

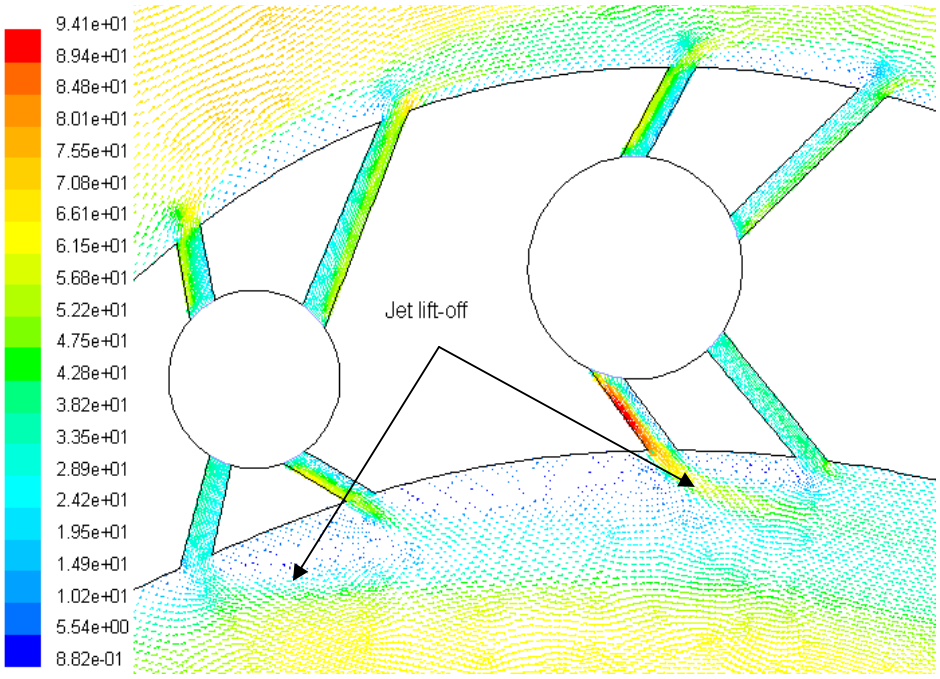

Fig. 4.13: Velocity vectors in the leading edge and core region of the pressure and suction side; blowing ratio, M=1(velocity magnitudes in m/s).

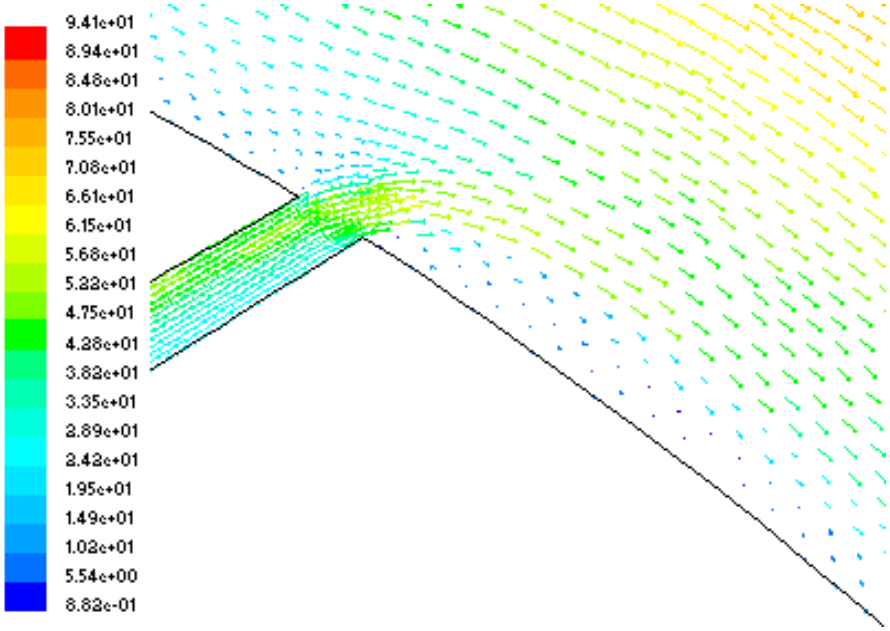

Fig. 4.14: Velocity vectors on the trailing edge of the suction side blowing ratio, M=1(velocity magnitudes in m/s).

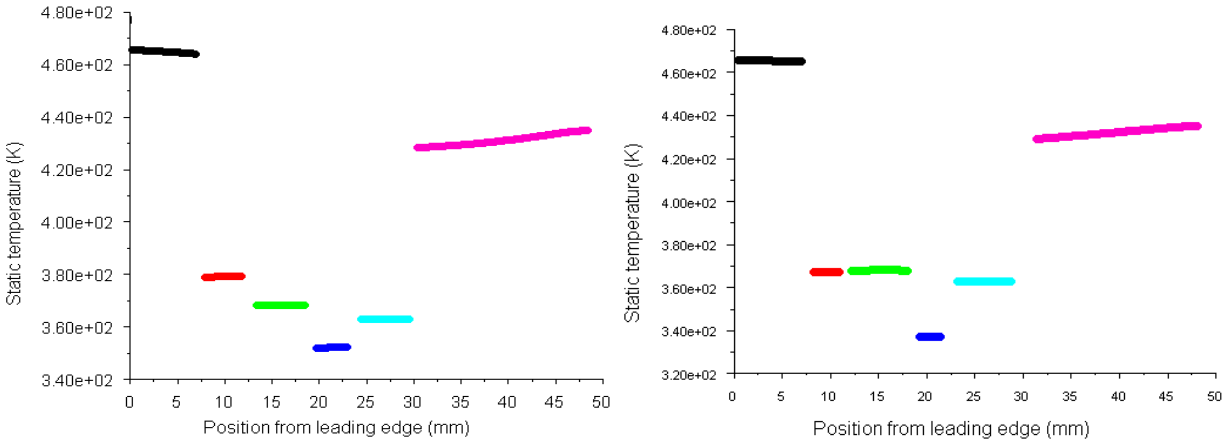

(a) Suction side; blowing ratio, M = 0.18 (b) Pressure side; blowing ratio, M = 0.18

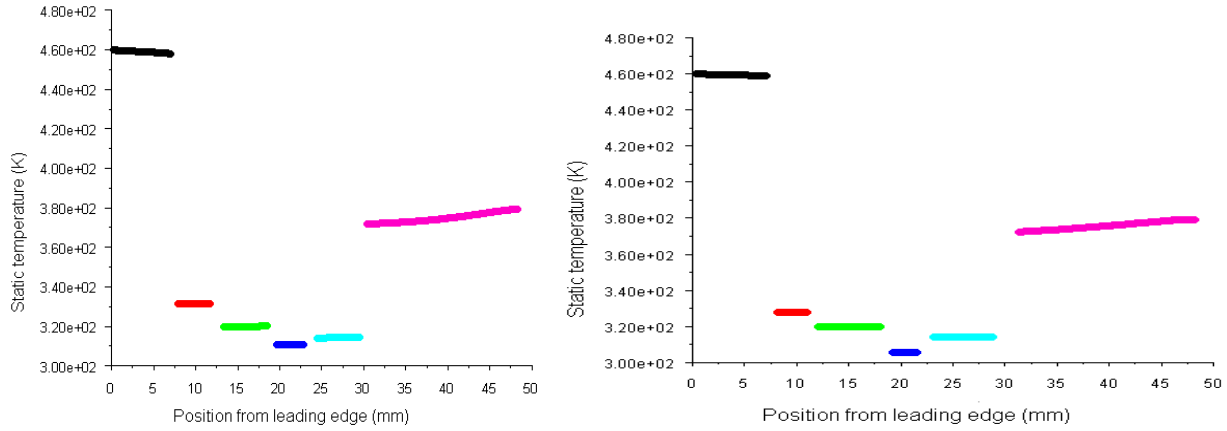

(c) Suction side; blowing ratio M = 0.5 (d) Pressure side; blowing ratio, M = 0.5

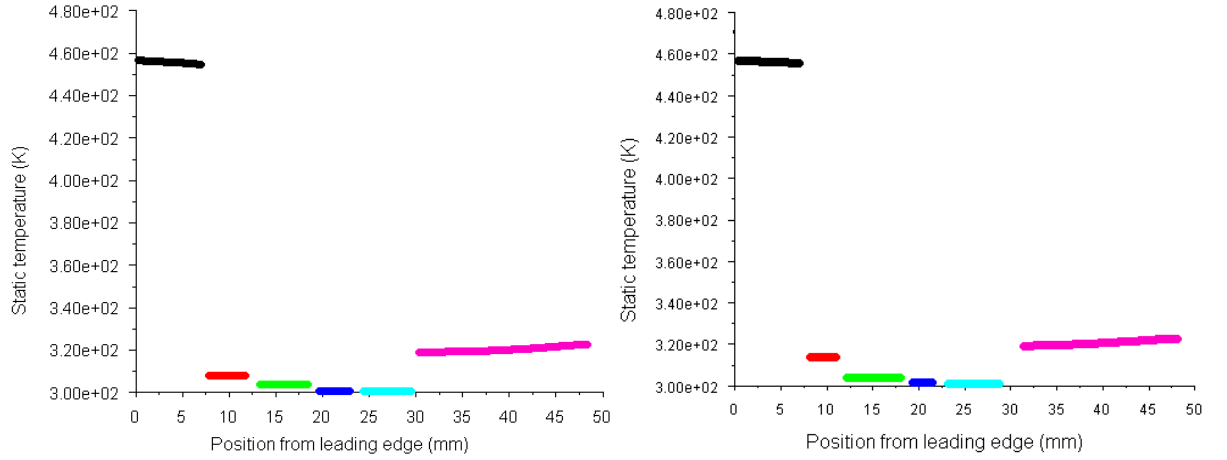

(e) Suction side; Blowing ratio, M = 1 (f) Pressure side; Blowing ratio, M = 1

Fig. 4.15: Temperature variation of the suction and pressure sides of the fan-shaped holes at three blowing ratios.

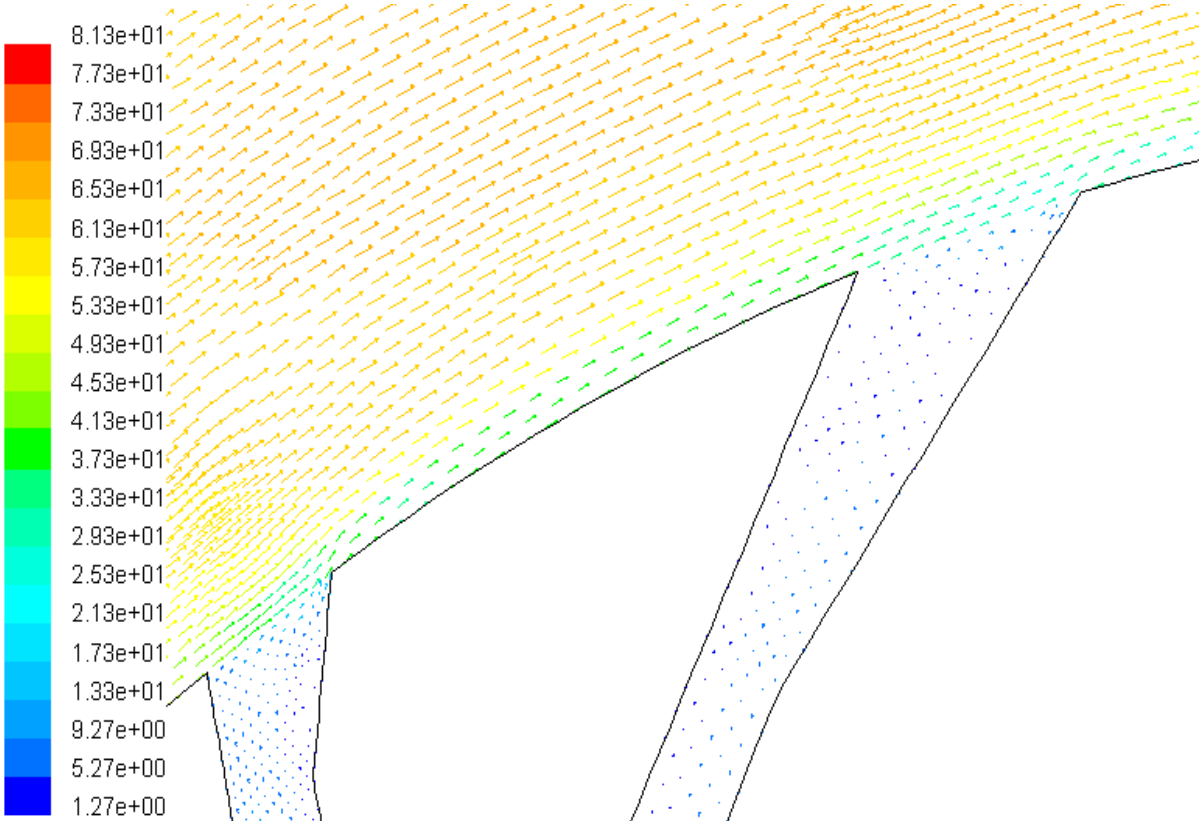

Fig. 4.16: Velocity vectors on the suction side; low blowing ratio, M = 0.18; velocity magnitudes in m/s. (Fan-shaped holes)

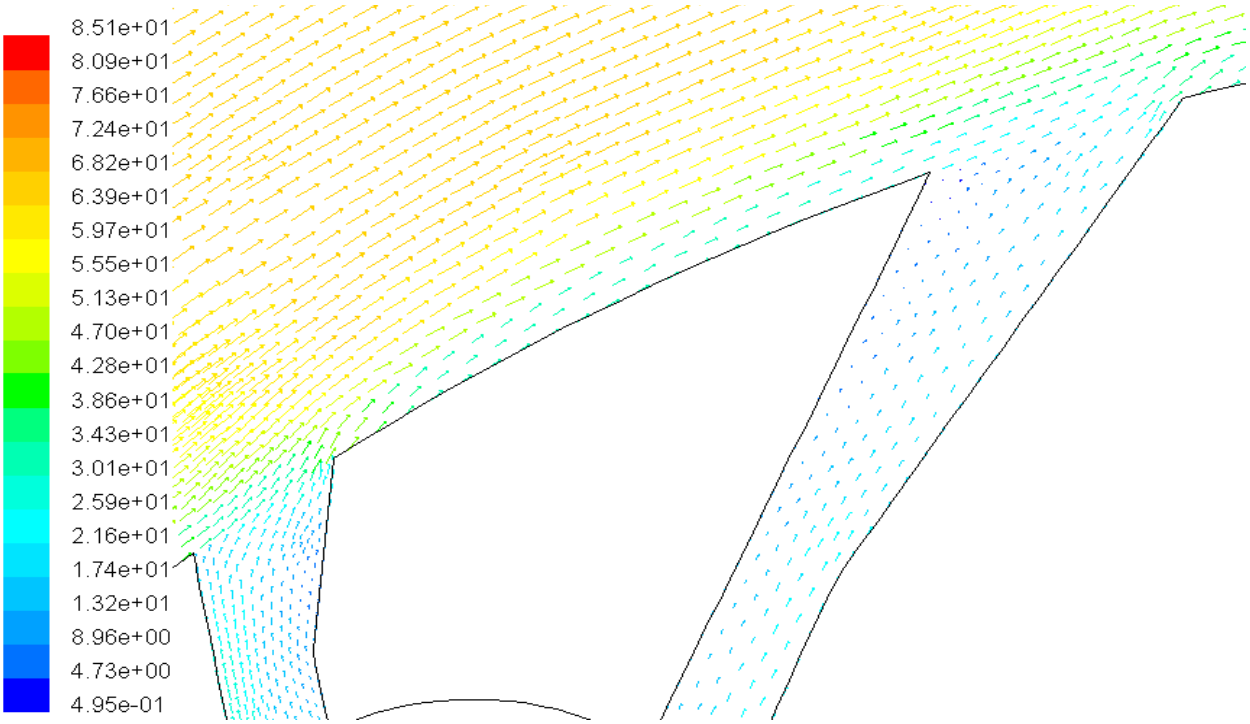

Fig. 4.17: Velocity vectors on the suction side; moderate blowing ratio, M = 0.50; velocity magnitudes in m/s. (Fan-shaped holes)

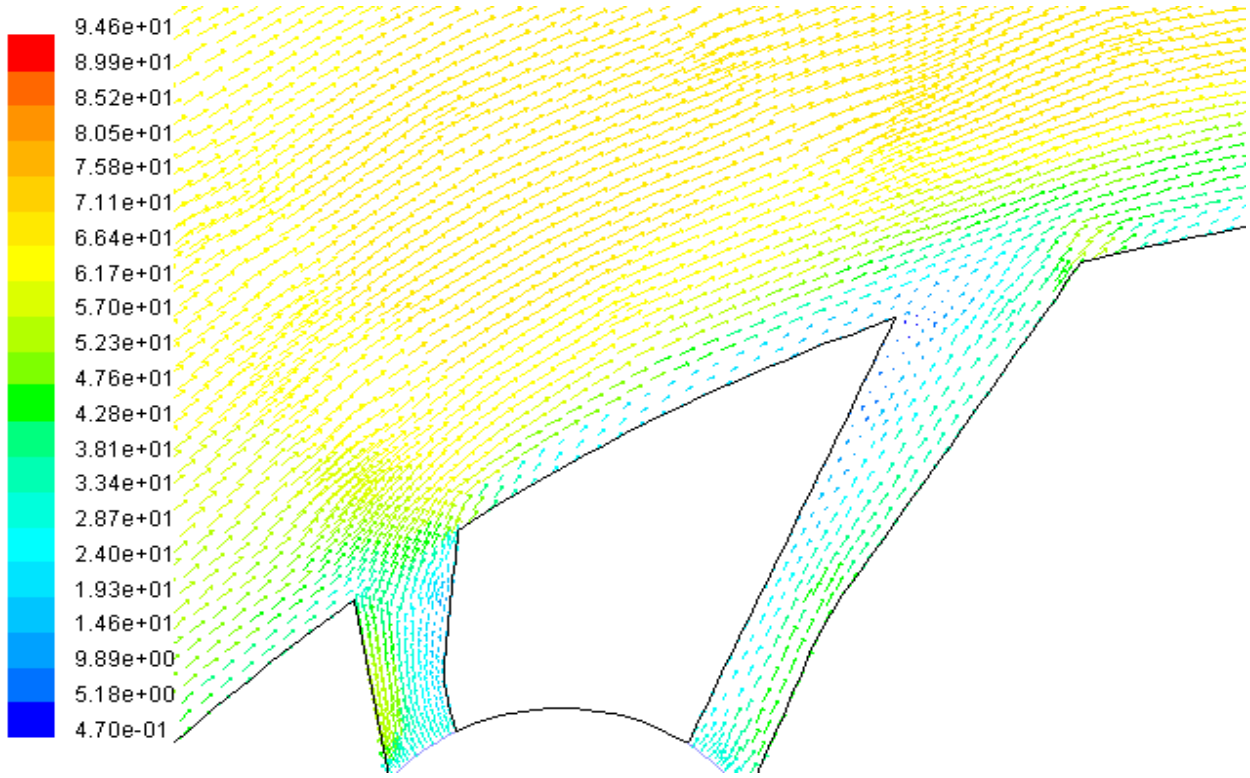

Fig. 4.18: Velocity vectors on the suction side; high blowing ratio, M = 1.0; velocity magnitudes in m/s.

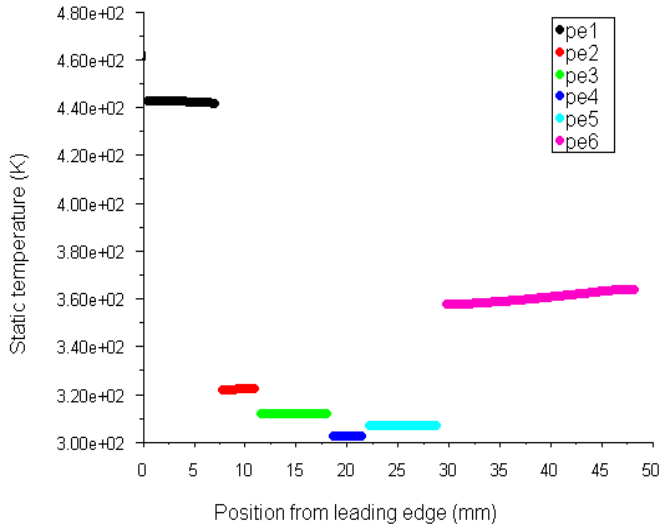

(a) Turbulence intensity, Tu=15%

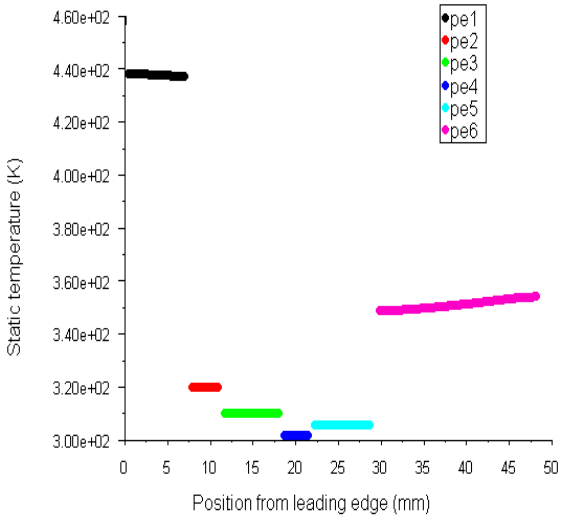

(b) Turbulence intensity, Tu=7%

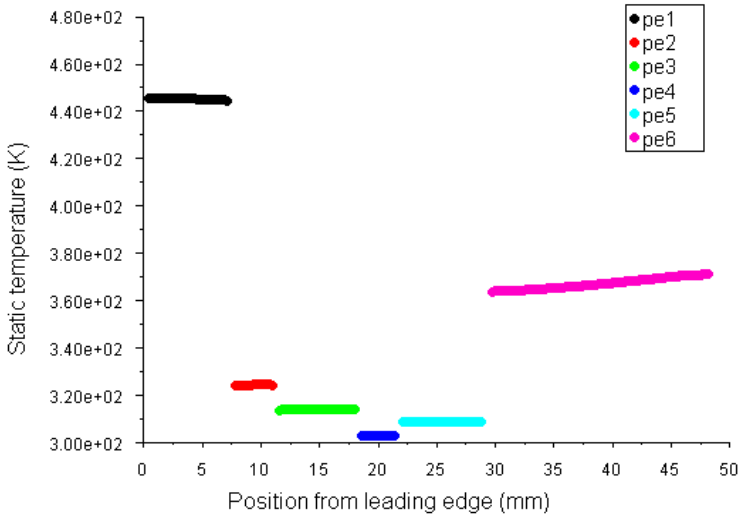

(c) Turbulence intensity, Tu=20%

Fig.4.19: Comparison of temperature distribution of the pressure side for cylindrical hole for different turbulence intensity: blowing ratio, M=0.5.

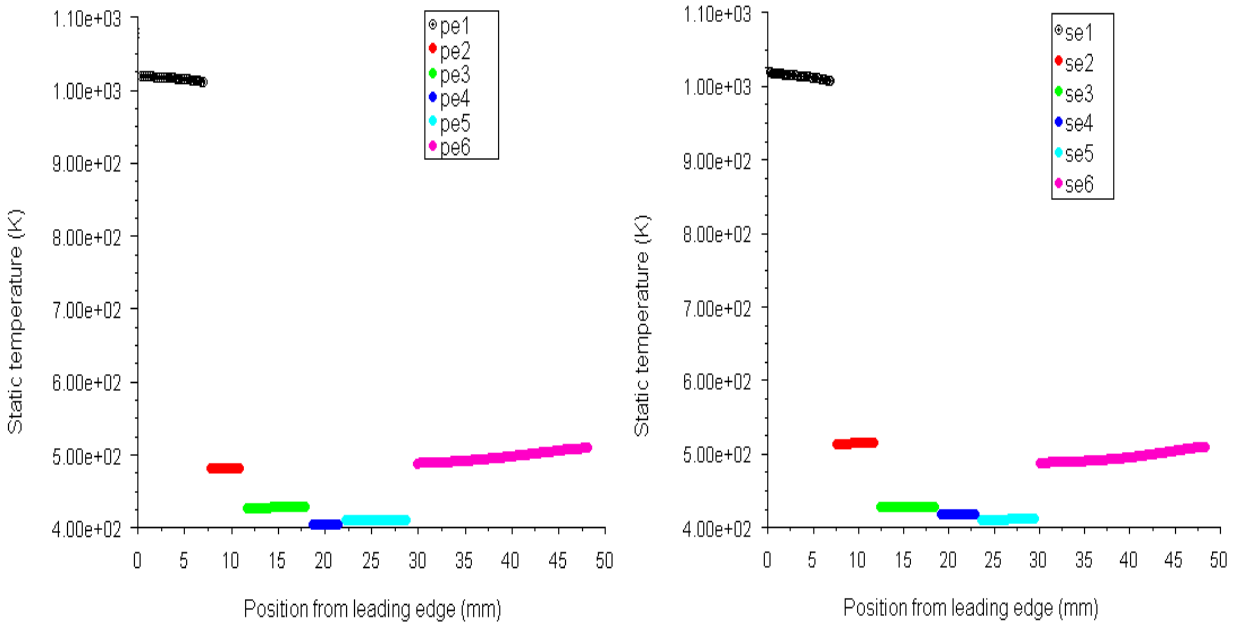

Fig. 4.20: Temperature distribution on the pressure and suction sides at turbine inlet temperature, T = 1100 K; blowing ratio, M = 0.5

This study presented a detailed computational investigation of film cooling on a gas turbine vane with simple cylindrical and fan-shaped holes for low, moderate and high blowing ratio. CFD predictions using the RNG κ- ε turbulence model was done. For various blowing rates the temperature and flow fields around the blade and inside the cooling hole were predicted. Flow and temperature field of the cooled vane were compared with that of the uncooled one. Results showed distortions of the mainstream gas due to its interaction with the coolant jet.

The flow and temperature field and their dependence on the blowing ratio, injection angle, length to diameter ratio appeared to be reasonably well predicted. A quantitative validation could not be made because of the absence of investigations on two dimension model.

Different arrangements of the cooling holes were investigated on the pressure side and suction side. It was observed that the hydrodynamics of the jets i.e., interactions of jets issuing from different rows of holes, can enhance or lower the film-cooling protection, as a function of the arrangement of the holes. This is due to the flow distortions through the passage induced by the lift-off of the film cooling jet.

For cylindrical holes, at low blowing ratio, similar temperature profiles were predicted for the pressure and suction side. Temperatures at the pressure side are 10-50^{o} higher than the suction side. Jet lift-off is minimal at the low blowing ratio. As the blowing ratio increased, temperature of the blade reduced further, while the flow field showed enhanced jet lift-off and mixing due to higher momentum flux ratio. For high

blowing ratio at the leading edge, severe turning of the coolant jet occurred leading to reversal of flow of the coolant. At the trailing edge because of lower injection angle, jet remained attached to the blade edge leading to a better cooling performance.

Fan-shaped holes showed reduction in cooling performance as compared to cylindrical holes at low blowing ratio due to very low velocity of the jet. But as the blowing ratio increased, they performed better than the cylindrical holes because of lower jet lift-off.

The effect of turbulence is not captured well which is supposed to impact the cooling performance. The blade temperature increased when the turbine inlet temperature was raised from 500 K to 1100 K.

Scope for future work

As there is a large variation in the spanwise direction, a three dimension model is always far more accurate for film-cooling flow predictions. This can be done by four or more parallel processors. The parallel processing technique is described well in Fluent documentation file. The effect of surface roughness of the vane can also be studied. The study can be extended to compound angle cylindrical holes (only possible in 3D) and laidback fan-shaped holes.

[1] Stefan Bernsdorf, Martin G. Rose Reza S. Abhari; 2008; **"**Experimental Validation of Quasisteady Assumption in Modeling of Unsteady Film-Cooling"; ASME J. Turbomach;**130**

[2] Karsten Kusterer, Dieter Bohn; "Double-Jet Ejection of Cooling Air for Improved Film Cooling"; ASME J. Turbomach;**129**

[3] Yoji Okita, Masakazu Nishiura**;** 2007; **"**Film Effectiveness Performance of an Arrowhead- Shaped Film-Cooling Hole Geometry"; ASME J. Turbomach;**129**

[4] Andre Burdet; Reza S. Abhari; 2007; "Three-Dimensional Flow Prediction and Improvement of Holes Arrangement of a Film-Cooled Turbine Blade Using a Feature-Based Jet Model"; ASME J. Turbomach; **129**

[5] Scot K. Waye; David G. Bogard; 2007; "High-Resolution Film Cooling Effectiveness Comparison of Axial and Compound Angle Holes on the Suction Side of a Turbine Vane"; ASME J. Turbomach; **129**

[6] W. Colban; K. A. Thole; 2007; "Experimental and Computational Comparisons of Fan-Shaped Film Cooling on a Turbine Vane Surface"; ASME J. Turbomach; **129**

[7] P. Martini; A. Schulz; H. J. Bauer; C. F. Whitney, 2006, "Detached Eddy Simulation of Film Cooling Performance on the Trailing Edge Cutback of Gas Turbine Airfoils" ; ASME J. Turbomach; **128**

[8] James L. Rutledge; David Robertson; David G. Bogard; 2006; "Degradation of Film Cooling Performance on a Turbine Vane Suction Side due to Surface Roughness"; ASME J. Turbomach; **128**

[9] W. Colban; A. Gratton; K. A. Thole; M. Haendler; 2006**; "**Heat Transfer and Film-Cooling Measurements on a Stator Vane With Fan-Shaped Cooling Holes"; ASME J. Turbomach; **128**

[10] P. Martini; A. Schulz; H.J. Bauer; 2006; "Film Cooling Effectiveness and Heat Transfer on the Trailing Edge Cutback of Gas Turbine Airfoils with Various Internal Cooling Designs"; ASME J. Turbomach; **128**

[11] Giovanna Barigozzi; Giuseppe Benzoni Giuseppe Franchini Antonio Perdichizzi; 2006; “Fan-Shaped Hole Effects on the Aero-Thermal Performance of a Film-Cooled Endwall”; ASME J. Turbomach; **128**

[12] Michael Gritsch; Will Colban Heinz; Schär Klaus Döbbeling; 2005; Effect of Hole Geometry on the Thermal Performance of Fan-Shaped Film Cooling Hole; ASME J. Turbomach; **127**

[13] Christian Saumweber; Achmed Schulz; Sigmar Wittig; 2003; Free-Stream Turbulence Effects on Film Cooling with Shaped Holes; ASME J. Turbomach; **125**

[14] J. Dittmar,A. Schulz, S. Wittig; 2003; “Assessment of Various Film-Cooling Configurations Including Shaped and Compound Angle Holes Based on Large-Scale Experiments” ASME J. Turbomach.; **125**

[15] D. K. Walters; J. H. Leylek; 2000; A Detailed Analysis of Film- Cooling Physics: Part I— Streamwise Injection with Cylindrical Holes; ASME J. Turbomach.; **122**

[16] D. G. Hyams; J. H. Leylek; 2000; A Detailed Analysis of Film Cooling Physics: Part III— Streamwise Injection With Shaped Holes; ASME J. Turbomach.; **122**

[17] E. Lutum; B. V. Johnson; 1999; Influence of the Hole Length-to- Diameter Ratio on Film Cooling With Cylindrical Holes; ASME J. Turbomach.; **121**

[18] Kohli, A., and Bogard, D., 1999, “Effects of Hole Shape on Film Cooling with Large Angle Injection,” ASME J. Turbomach.; **121**.

[19] Thole, K. A., Gritsch, M., Schulz, A., and Wittig, S., 1998, “Flowfield Measurements for Film-Cooling Holes With Expanded Exits,” ASME J. Turbomach.,**120**

[20] H. H. Cho; R. J. Goldstein; 1995; Heat (Mass) Transfer and Film Cooling Effectiveness with Injection through Discrete Holes: Part I—Within Holes and on the Back Surface; ASME J. Turbomach.; **117**

[21] H. H. Cho; R. J. Goldstein; 1995; Heat (Mass) Transfer and Film Cooling Effectiveness with Injection through Discrete Holes: Part II— on the Exposed Surface; ASME J. Turbomach.; **117**

[22] Cohen, H; Rogers, GFC; Saravanamuttoo, HIH; 1996, Gas Turbine Theory, Longman Group Ltd.

[23] S. M. Yahya, 2007, “Turbines, Compressors and Fans”, Tata McGraw Hill.

[24] Lysbeth S. Lieber, 2006, 2nd Edition, Handbook of Turbomachinery.

[25] Nicholas P. Cheremisinoff, 2000, Encyclopedia of Fluid Mechanics, **1**: Flow Phenomena and Measurement; Gulf Pub Co.

[26] Omar Othman Badran; 1999; Gas-turbine performance improvements; Elsevier Science Ltd.

[27] www. Inrnews.com

[28] www.indiastat.com

[29] www.cslforum.com

[30] www.wikipedia.com

[31] www.vki.ac.be

APPENDIX – 1

GLOSSORY OF TERMS

Aspect ratio

Ratio of blade height to chord. If aspect ratio is reduced the contribution of secondary losses in total losses increases.

Blade angle

Included angle between tangents drawn on the camber line at leading edge and trailing edge with the axial or tangential direction are the blade angles at inlet and exit, respectively.

Camber angle

The angle between tangent drawn on the camber line at leading edge and chord line at inlet, the angle between tangent drawn on the camber line at trailing edge and chord line is camber angle at exit. The sum of camber angle at inlet and exit is camber angle.

Camber line

A blade section of infinitesimal thickness is a curved line known as camber line. This forms the backbone line of a blade of finite thickness.

Cascade

An infinite row of equidistant similar blade is called a cascade. When blades are arranged in a straight line the cascade is called rectilinear cascade. In annular cascades, the blades are arranged in an annulus. In a radial cascade the blades are arranged radial inward or outward direction.

Chord

A straight line joining center of leading edge and center of trailing edge. The length of this line is blade chord.

Deviation

The difference between flow angle and blade angle at outlet is called deviation angle. It also may be positive or negative.

Flow inlet angle

Angle that the flow makes at inlet with the axial or tangential direction.

Flow outlet angle

Angle that the flow makes at outlet with the axial or tangential direction. It depends on pitch-chord ratio and stagger angle.

Incidence angle

The difference between flow angle and blade angle at inlet. It may be positive or negative.

Leading edge thickness

Edge of Blade where the flow enters.

Pitch-cord ratio

Ratio of pitch to the chord

Pressure and suction surface

The concave surface of the blade is called pressure surface, and convex surface is called suction surface.

Span

Height of the blade from hub to tip.

Stagger angle

Stagger angle is the inclination of chord line with the axial or tangential direction. The shape of the channel changes with change in stagger angle, which results in change in pressure distribution and boundary layer thickness and hence losses. Increase in stagger angle (axial) increases semi-vane-less region and reduces the throat. For the same stagger angle exit angle changes with pitch-chord ratio and for pitch-chord ratio exit angle increase with increase in stagger angle.

Injection angle: -

The angle measured between the streamwise direction and the tangent at the outlet of the hole.

Hole-pitch: -

Distance between two holes in streamwise or spanwise direction.

APPENDIX – 2

Coordinates of the profile 6030

x	y	x	y	x	y
0.17	2.29	49.90	0.86	5.93	3.77
0.18	2.37	50.00	0.67	4.98	2.98
0.22	2.55	50.06	0.54	4.25	2.36
0.42	3.38	50.06	0.42	3.40	1.62
0.67	4.19	50.02	0.28	2.76	1.07
1.23	5.67	49.97	0.24	2.40	0.76
1.71	6.79	49.94	0.23	2.24	0.62
2.41	8.14	49.91	0.22	1.79	0.23
2.83	8.88	49.86	0.21	1.41	-0.09
3.93	10.69	49.72	0.20	0.83	-0.19
4.98	12.01	49.52	0.29	0.56	-0.16
6.38	13.43	49.28	0.41	0.35	-0.09
7.15	14.13	49.09	0.53	0.21	0.01
8.32	15.04	48.80	0.71	-0.01	0.22
9.51	15.80	48.52	0.89	-0.07	0.66
10.88	16.55	48.04	1.21	0.01	1.44
12.68	17.34	47.43	1.60	0.09	1.87
14.16	17.79	46.50	2.18	0.17	2.29
19.70	18.54	43.69	3.88		
21.15	18.47	41.80	4.95		
22.78	18.28	39.99	5.93		
25.04	17.89	38.54	6.68		
27.29	17.19	36.82	7.51		
29.35	16.33	35.45	8.12		
30.28	15.92	34.05	8.67		
32.09	15.02	31.98	9.42		
34.41	13.69	29.72	10.00		
36.75	12.12	27.63	10.31		
38.82	10.60	26.63	10.41		
40.07	9.62	25.37	10.50		
41.96	8.07	24.12	10.52		
43.82	6.45	22.44	10.47		
46.00	4.49	20.99	10.35		
47.35	3.26	18.50	10.00		
48.23	2.47	16.58	9.55		
48.66	2.07	14.99	9.04		
48.93	1.83	13.93	8.68		
49.11	1.66	11.48	7.67		
49.28	1.49	9.21	6.26		

APPENDIX - 3

Details of model used: -

A3.1 Meshing at a glance: -

A3.1.a Uncooled blade: -

Number of cells	40,694
Number of faces	82,323
Number of nodes	42,524
Number of zones	8
Number of continuums	2
Type of cell	Quadrilateral
Method of meshing	Pave

A3.1.b Simple cylindrical holes

Number of cells	74,309
Number of faces	1,50,853
Number of nodes	76,508
Number of zones	28
Number of continuums	2
Type of cell	Quadrilateral
Method of meshing	Pave

A3.2.c Fan-shaped holes

Number of cells	75,875
Number of faces	1,53,807
Number of nodes	77,896

Number of zones	28
Number of continuums	2
Type of cell	Quadrilateral
Method of meshing	Pave

A3.2 Fluent model at a glance: -

Model	**Setting**
Version	2DDP
Time	Steady
Viscous	RNG k-ε turbulence model
Wall treatment	Standard wall functions
Energy equation	Enabled
Solidification and melting	Disabled
Radiation	Disabled
Species transport	Disabled
Pollutants	Disabled

A3.3 Solver Control

(a) Equation solved

Equations	**Solved**
Flow	Yes
Turbulence	Yes
Energy	Yes

(b) Relaxation

Variable	Relaxation factor
Pressure	0.3
Density	1.0
Body force	1.0
Momentum	0.7

(c)Discretization scheme

Variable	Scheme
Pressure	Standard
Pressure velocity compounding	Simple
Density	Second order upwind
Momentum	Second order upwind
Turbulence kinetic energy	Second order upwind
Turbulence dissipation rate	Second order upwind
Energy	Second order upwind

(e) Solution limits

Quantity	Limit
Minimum absolute pressure	1
Maximum absolute pressure	5000000
Minimum temperature	1
Maximum temperature	5000
Minimum turbulence kinetic energy	$1\times e^{-14}$
Minimum turbulence dissipation rate	$1\times e^{-20}$
Maximum turbulence viscosity rate	100000

A3.4 Material Property

(a) Material air (fluid)

Property	Units	Method	Value
Density	Kg/m^3	Incompressible Ideal gas	1.225
Specific heat (C_p)	J/kg-K	Constant	1006.43
Thermal conductivity	W/m-K	Constant	0.0242
Viscosity	Kg/m-s	Constant	1.7894e-0

(b) Material Aluminum (solid)

Property	Units	Method	Value
Density	Kg/m^3	Constant	2719
Specific heat (C_p)	J/kg-K	Constant	871
Thermal conductivity	W/m-K	Constant	202.4

A3.5 Convergence criteria

Continuity	$1\times e^{-06}$
X-velocity	$1\times e^{-06}$
Y-velocity	$1\times e^{-06}$
Energy	$1\times e^{-06}$
Turbulence kinetic energy (k)	$1\times e^{-06}$
Turbulence dissipation rate (ε)	$1\times e^{-06}$

A3.6 Total time for Convergence (min.)

Uncooled Blade	Simple Cylindrical	Fan-shaped
~15	~25	~28